

# **Optical Inspection of Industrial Product**

Optická kontrola průmyslového výrobku

**Juliana Maya Boscan**

Diploma Thesis

Supervisor: doc. Ing. Petr Bilík, Ph.D.

Ostrava, 2021

## **Abstract**

The implementation of algorithms based on computer vision to the industry has brought great advantages when carrying out inspections of industrial products, that is why this document focuses on the realization of a 3D inspection of an object through the method of Photometric Stereo. A method that is based on taking images under different lighting directions, thus allowing estimating the map of the surface of the object under inspection. To develop this method, a light ring from the Smart Light company with its respective controller and a Basler monochrome camera was implemented.

During the development of this master's thesis, it was possible to observe the operation of each of the stages to carry out the inspection, in this case, the capture of images, the reconstruction method, and the calibration process to convert pixels to real units and thus to be able to compare the dimensions obtained by the algorithm concerning the real measurements of the object. Finally, the response of the system to objects that differ from one another concerning geometry, size, or material is analyzed and thus the precision of the approach used is verified.

## **Keywords:**

Photometric stereo, Lambertian surface, Normal surface, Surface Albedo, Depth map, Camera, Ring light, Pixel.

## **Abstrakt**

Implementace algoritmů založených na počítačovém vidění v průmyslu přinesla velké výhody při provádění inspekci průmyslových produktů, proto se tento dokument zaměřuje na realizaci 3D inspekce objektu metodou fotometrického sterea. Metoda, která je založena na pořizování snímků v různých směrech osvětlení, což umožňuje odhadnout mapu povrchu kontrolovaného objektu. K vývoji této metody byl využit segmentový prstencový osvětlovač od společnosti Smart Light s příslušným ovladačem a monochromatickou kamerou Basler.

Během vývoje této diplomové práce je možné sledovat provoz každé z fází provádění kontroly, v tomto případě pořizování snímků, metodu rekonstrukce a proces kalibrace pro převod pixelů na skutečné jednotky, a tak být schopen porovnat rozměry získané algoritmem týkajícím se skutečných měření objektu. Nakonec je analyzována odezva systému na objekty, které se navzájem liší, pokud jde o geometrii, velikost nebo materiál, a ověřuje se tak přesnost použitého přístupu.

## **Klíčová slova:**

Fotometrické stereo, Lambertovský povrch, Normální povrch, Odrazivost povrchu, Hloubková mapa, Kamera, Prstencový osvětlovač, Pixel.

## **Acknowledgment**

This master's thesis would not have been possible without the support of many wonderful people who took their time to help me and guide me to complete it. First, I want to thank God for bringing me here and every day to give me the strength and wisdom necessary to complete this master's thesis. Many thanks to my supervisor Petr Bilik for trusting me and making me a better professional every day, for his patience and advice.

Thanks to my mother, my father, my sister, and my brothers for reminding me daily that dreams are here to come true and to be my support during this journey.

I also want to thank two people who, more than cousins, are brothers, Carmen and Kiko, thank you very much for your support because without you I would not be the Electronic Engineer that I am now.

My friend Arley, thanks for the late nights trying to discuss each of the points that make up this thesis, and thanks to the best friend JuanCa for keeping me company during the night work.

Finally, many thanks to my big brothers Nabil and Jan for their support, for trusting me, and for each piece of advice that has made me grow both professionally and personally.

# Content

Abbreviations .....	6
List of figures .....	7
List of tables .....	9
List of equations .....	10
Introduction.....	11
1. Analysis of image processing in industrial visual inspections .....	12
1.1. Description of a general image processing system .....	12
1.2. Cameras usage on an industrial vision system.....	15
1.2.1. Types of sensors implemented on cameras .....	15
1.2.2. Classification of smart cameras implemented on artificial vision.....	17
1.2.3. Camera lenses and filters .....	19
1.2.4. Camera interface .....	20
1.3. Illumination using an industrial vision system .....	21
1.3.1. Type of light concerning wavelength .....	21
1.3.2. Light sources.....	22
2. Description of the development environments and development technologies used in the visual inspection of industrial product .....	25
3. Theoretical analysis of 3D reconstruction with Photometric Stereo approach .....	28
3.1. Lighting .....	28
3.2. Phenomena of reflectance .....	29
3.2.1. Analysis of a surface reflectance .....	30
3.2.2. Bidirectional reflectance distribution function .....	31
3.3. Lambertian reflectance model .....	32
3.3.1. Surface Albedo .....	34
3.3.2. Normal surface .....	34
3.3.3. Depth map.....	35
3.4. Shape from shading procedure .....	36
3.5. Photometric stereo .....	37
3.5.1. Mathematical description .....	38
4. Design of an inspection of industrial product .....	39
4.1. Requirements for optical inspection.....	39
4.2. Description of the solution.....	40

4.3.	Components for the optical evaluation.....	42
4.3.1.	Camera .....	43
4.3.2.	Illumination .....	45
5.	Software design for the visual inspection of industrial product .....	47
5.1.	Image acquisition program.....	47
5.2.	3D reconstruction algorithm .....	49
5.3.	Light direction calculation .....	52
5.4.	Camera calibration .....	54
5.4.1.	Pixel to real unit conversion for X and Y-axis .....	56
5.4.2.	Pixel to real unit conversion for Z-axis .....	57
6.	Evaluation of the achieved results .....	59
	Conclusion .....	63
	References.....	64

## Abbreviations

<b>2D</b>	Bidimensional or Two Dimensions
<b>3D</b>	Tridimensional or Three Dimensions
<b>BRDF</b>	Bidirectional Reflectance Diffuse Function
<b>SFS</b>	Shape From Shading
<b>PS</b>	Photometric Stereo
<b>HW</b>	Hardware
<b>SW</b>	Software
<b>LABVIEW</b>	Laboratory Virtual Instruments Engineering Workbench
<b>ASIP</b>	Application-Specific Information Processing
<b>MOS</b>	Metal-Oxide-Semiconductor sensors
<b>CCD</b>	Charge-Coupled Device
<b>CMOS</b>	Complementary Metal-Oxide-Semiconductor
<b>IR</b>	Infrared
<b>UV</b>	Ultraviolet
<b>FPGA</b>	Field-Programmable Gate Array
<b>DSP</b>	Digital Signal Processor
<b>LED</b>	Light Emitting Diodes
<b>W</b>	Watts
<b>m</b>	Meters
<b>sr</b>	Stereoradians
<b>lx</b>	Lux

## List of figures

Figure 1 - Description of an industrial vision system. [4] .....	12
Figure 2 - Common image processing system .....	12
Figure 3 - Image acquisition model. [5] .....	13
Figure 4 - Example of a morphological segmentation process, (a) Source image, (b) Threshold, (c) Distance, (d) Watershed, and (e) Result image .....	14
Figure 5 - Feature extraction model .....	14
Figure 6 - Example of an optical inspection. ....	15
Figure 7 - The structure of a typical smart camera. ASIP: Application-Specific Information Processing. [6] .....	15
Figure 8 - Light to voltage conversion difference between CCD and CMOS sensors. [7] .....	16
Figure 9 - Classification of smart cameras implemented on artificial vision. [6] .....	17
Figure 10 - Example of Smart cameras: Sony XCI-SX1 smart camera for machine vision applications (left photo); Intellio ILC-210 smart camera for security and surveillance applications (right photo). [6] .....	17
Figure 11 - Example of a Single-chip smart camera (VISoc Chip: NN-vision/neural processor, S-sensor, R-RISC processor). [8] .....	18
Figure 12 - Example of distributed smart camera's structure (subject captured by a distributed smart camera system) [9] .....	19
Figure 13 - Generic interface of a camera. [10] .....	20
Figure 14 – Part of the electromagnetic spectrum. [11] .....	22
Figure 15 - Emission spectra of different light sources. [12] .....	22
Figure 16 - Structure of incandescent lamps. [13] .....	23
Figure 17 - Example of a structure of a fluorescent lamp. [14] .....	23
Figure 18 - Structure of a light-emitting diode. [15] .....	24
Figure 19 - Object inspection example developed in LabVIEW .....	25
Figure 20 - Example of a block diagram created in LabVIEW .....	26
Figure 21 - Model of image formation. [17] .....	28
Figure 22 - Description of a point light source. ....	28
Figure 23 - Description of the inverse square law. [18] .....	29
Figure 24 - Description of an area light source. ....	29
Figure 25 - Diagram of the law of reflection. [20] .....	30
Figure 26 - Specular and diffuse reflection from an object surface. [1] .....	30
Figure 27 - Specular reflection. [17] .....	30
Figure 28 - Example of specular and diffuse reflection under the same light source and same spherical object. [1] .....	31
Figure 29 - (a) Example of light scatters, (b) The bidirectional reflectance distribution function. [17] .....	31
Figure 30 - The reduction of reflected light caused by the foreshortening factor varies on, the cosine of the angle between the incident light direction and the normal surface. [17] .....	32
Figure 31 - Vectors for modeling BRDFs. [3] .....	32
Figure 32 - Lambertian reflection model. [21] .....	33
Figure 33 - (a–d) Images acquired at different illumination directions, (e) Surface normal image, (f) albedo map, and (g) Reconstructed 3D image. [23] .....	34
Figure 34 - Explanation of how the normal vector (N) is formed from the incident light (L). [1] .....	34
Figure 35 - Relationship between Cartesian coordinates and image coordinates. [24] .....	35

Figure 36 - Example of a depth map. [25] .....	35
Figure 37 - Principle of photometric stereo. a) Intensity of the object when the surface is flat and normal to the camera. b) Intensity of an uneven object [1]. .....	37
Figure 38 - Example of schematics for Photometric stereo model. [27].....	37
Figure 39 - Location of the lighting system (Necessary parameter to build the lighting vector - $Ln$ ). [1]..	38
Figure 40 - Example of 3D reconstruction result using photometric stereo.....	39
Figure 41 – Main blocks for the project solution. ....	40
Figure 42 - Procedure for image acquisition. ....	41
Figure 43 - Pipeline of the reconstruction program.....	42
Figure 44 – Physical diagram of the solution model. ....	43
Figure 45 - Basler ace GigE acA1300-30gm camera. [28].....	44
Figure 46 - Ring smart light. [29] .....	45
Figure 47 - The user application for setting the ring light parameters. ....	46
Figure 48 - Activity diagram of image acquisition. ....	47
Figure 49 - Panel for activating the process of taking pictures. ....	48
Figure 50 - USB configuration Panel.....	48
Figure 51 - Timing diagram for image acquisition.....	49
Figure 52 - Activity diagram for 3D reconstruction program. ....	50
Figure 53 - 3D reconstruction program designed in LabVIEW. ....	52
Figure 54 - Fitting light probe circle. ....	52
Figure 55 - Finding light direction.....	53
Figure 56 - Graphic representation of the sphere with a highlight at point H.....	54
Figure 57 - Chessboard pattern.....	54
Figure 58 - Camera projection model.....	55
Figure 59 - Extrinsic parameters visualization.....	55
Figure 60 - Detected and reprojected points from chessboard pattern.....	56
Figure 61 - Process of conversion from pixel to real units.....	57
Figure 62 - Real height measured.....	57
Figure 63 - Z-axis after multiplying by the scale factor (X and Y axis are calibrated).....	58
Figure 64 - Example of how the measurement of the real measure was performed.....	59



## List of tables

Table 1 - Operations performed during image processing. [4] .....	13
Table 2 - Wired communication protocols. [6] .....	21
Table 3 – Some function blocks implemented on vision applications. [16] .....	27
Table 4 - Some criteria to design an image processing model.....	40
Table 5 - Camera parameters. [28].....	44
Table 6 - Ring light parameters. [29] .....	45
Table 7 - 3D reconstruction for a pyramid with dimensions of 50mm x 50mm x 25mm. ....	59
Table 8 - 3D reconstruction for a pyramid with dimensions of 50mm x 50mm x 12,5mm. ....	60
Table 9 - 3D reconstruction for a cube with dimensions of 20mm x 20mm x 20mm.....	61
Table 10 - 3D reconstruction for a pyramid with dimensions of 20mm x 20mm x 10mm. ....	62

## List of equations

Eq. 1	Inverse-square law	28
Eq. 2	Bidirectional reflectance diffuse function	31
Eq. 3	Simplified bidirectional reflectance diffuse function	31
Eq. 4	Calculation of reflected light	32
Eq. 5	Foreshortening factor	32
Eq. 6	Calculation of reflected light from each pixel	33
Eq. 7	Intensity of reflection	33
Eq. 8	Reflectance characteristic on Lambertian surface	33
Eq. 9	Spectral Albedo	34
Eq. 10	Three-dimension points	35
Eq. 11	x coordinate depending on the image plane coordinate	35
Eq. 12	y coordinate depending on the image plane coordinate	35
Eq. 13	Normal surface	36
Eq. 14	Eikonal equation	36
Eq. 15	Auxiliary variable of $\frac{\partial z}{\partial u}$	36
Eq. 16	Auxiliary variable of $\frac{\partial z}{\partial v}$	36
Eq. 17	Depth map calculation	36
Eq. 18	Relation respecting surface gradient	36
Eq. 19	The relation between reflectance surface with the brightness map	36
Eq. 20	Reflectance characteristic on Lambertian surface (Matrix view)	38
Eq. 21	Normal surface calculation	38
Eq. 22	Photometric stereo equation with new variable assigned	50
Eq. 23	$G(x, y)$ equation	51
Eq. 24	Albedo calculation using $G(x, y)$	51
Eq. 25	Normal Surface calculation using $G(x, y)$	51
Eq. 26	Relation between normal surface respecting depth partial derivations	51
Eq. 27	Auxiliary variable p calculation	51
Eq. 28	Auxiliary variable q calculation	51
Eq. 29	Depth map calculation using Frankot and Chellappa method	51
Eq. 30	Highlight location calculation	53
Eq. 31	Normal vector in x location (Highlight)	53
Eq. 32	Normal vector in y location (Highlight)	53
Eq. 33	Normal vector in z location (Highlight)	53
Eq. 34	Error calculation	59

## Introduction

The industry is changing and consequently brings with it the implementation of new disciplines during the manufacturing process, which give the possibility to interact with manual processes with digital mechanisms to improve the quality of the products. One of those disciplines is computer vision, an approach normally used for acquiring, processing, and analyzing images to interpret the information and decide depending on resulting characteristics.

Computer vision is currently involved in different areas in the manufacturing field as predictive maintenance, product assembly, 3D inspection, and other activities. The scope of this diploma thesis was focused on the inspection of industrial products using 3D reconstruction, to obtain the shape and appearance of the object to be inspected.

Unlike the regular inspections that provide information from two dimensions, the 3D inspection is based on acquiring the height information from a collection of views and adding this information to a 2D image. Giving not just height information of the object but also sectional area and volume, improving the accuracy during the inspections and solving different problems that using 2D reconstruction was not able to solve, for example, inspecting the profile of solder.

Currently, different techniques allow 3D reconstructions, one of them is interferometry, a technique that sends waves with the same characteristics through the same medium, generating the interference phenomenon, a phenomenon that adds these waves and forms a new wave with different amplitude, where that amplitude is the sum of each superimposed wave. [1]

Another technique is structured illumination, implemented for example on a microscopical application, this procedure is based on the use of constructed light patterns that are projected on the surface or object. Therefore, when the light hits the surface, those patterns are deformed, allowing to obtain information about the surface, for example, the depth. [1]

In the field of autonomous vehicles, it is possible to see the implementation of the stereo vision technique, an alternative that allows 3D reconstruction. This method implements more than one camera in different positions, giving multiple images concerning the surface or object to be reconstructed when obtaining each image the purpose is to recognize the regions that share between the images to make the 3D reconstruction using the principle of triangulation and the regions that have no relationship help to give information about the depth of the object. [2]

Finally, the last procedure and the method implemented in this diploma thesis was photometric stereo, a technique that unlike stereo vision contains a camera in a defined position but the surface and depth are estimated by changing the position of the light that illuminates the object. [3]

# 1. Analysis of image processing in industrial visual inspections

In the production process, the implementation of image processing (See Figure 1) brings with it, different advantages during the assembly, manufacturing, and quality control phases of a product.

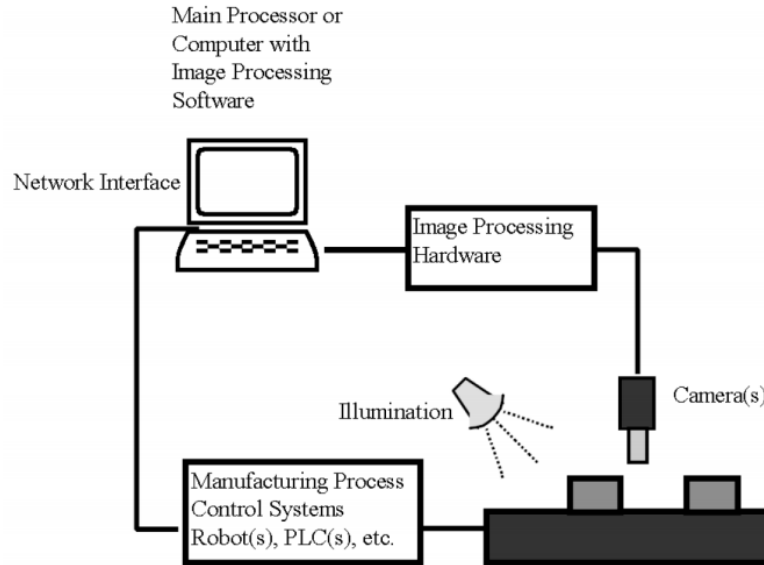


Figure 1 - Description of an industrial vision system. [4]

- The replacement of the operator by a control system capable of performing the final testing process using image processing algorithms ensures early detection of faults and defects, generating an increase in the reliability of inspections and avoiding possible rejections of the product by the customer.
- Optimize workflows and reduce costs due to manual tests and underutilization of production lines.

## 1.1. Description of a general image processing system

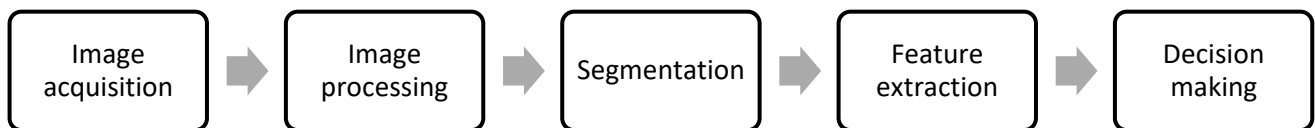


Figure 2 - Common image processing system.

### - Image acquisition

Image acquisition is the sub-process in charge of converting data from the real world (images) into numerical data that will be manipulated using a computer (see Figure 3).

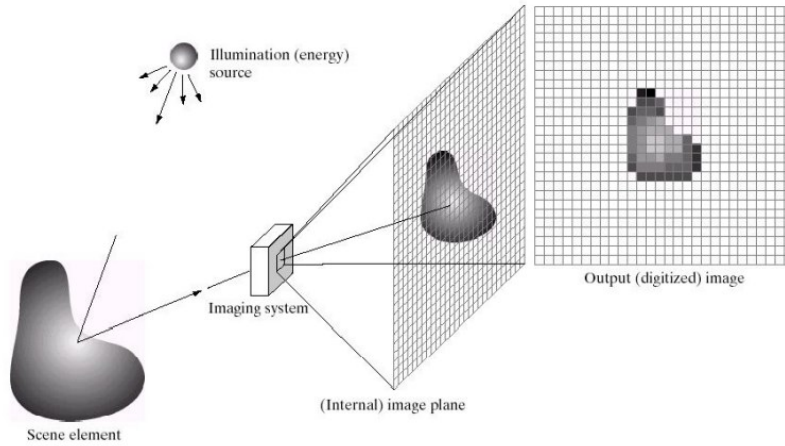


Figure 3 - Image acquisition model. [5]

- **Image processing**

During the development of this stage, the acquired images are prepared to implement different operations, to obtain a new image or a characteristic associated with the input image.

Table 1 - Operations performed during image processing. [4]

Point operations	Global operation	Neighborhood operation	Geometric operation	Temporal operation
Brightness modification	Histogram equalization	Image smoothing	Display adjustment	Frame-based operations
Contrast enhancement		Image sharpening	Image wrapping	
Negation and thresholding			Magnification and rotation	

- **Segmentation**

This step is responsible for dividing the input image into different segments (see the example in Figure 4), usually implemented in the location of objects.

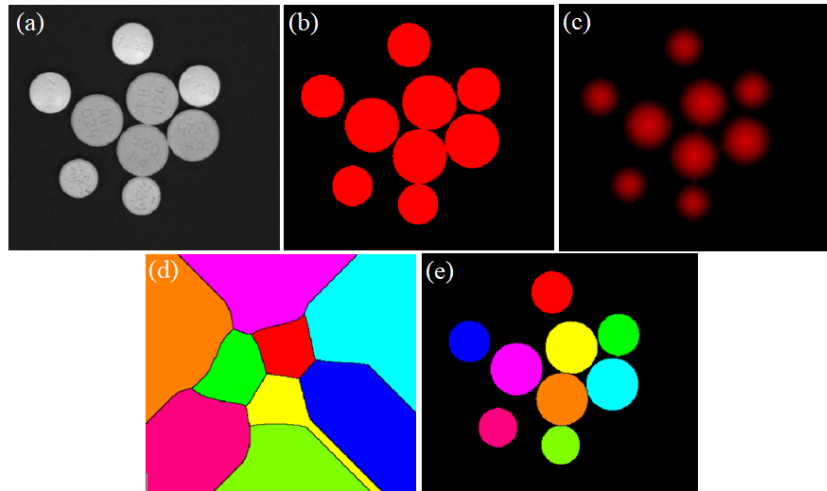


Figure 4 - Example of a morphological segmentation process, (a) Source image, (b) Threshold, (c) Distance, (d) Watershed, and (e) Result image.

- **Feature extraction**

Feature extraction consists of reducing the amount of information to describe a data set (see Figure 5). [4]

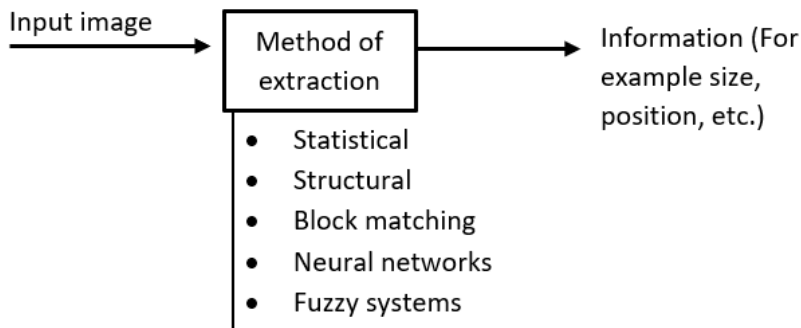


Figure 5 - Feature extraction model.

- **Decision making**

Decision-making is the last step in the image processing model, where depending on the application the process decides. For example, if the implemented process is an optical inspection (see Figure 6), the system results in whether the product meets quality standards.

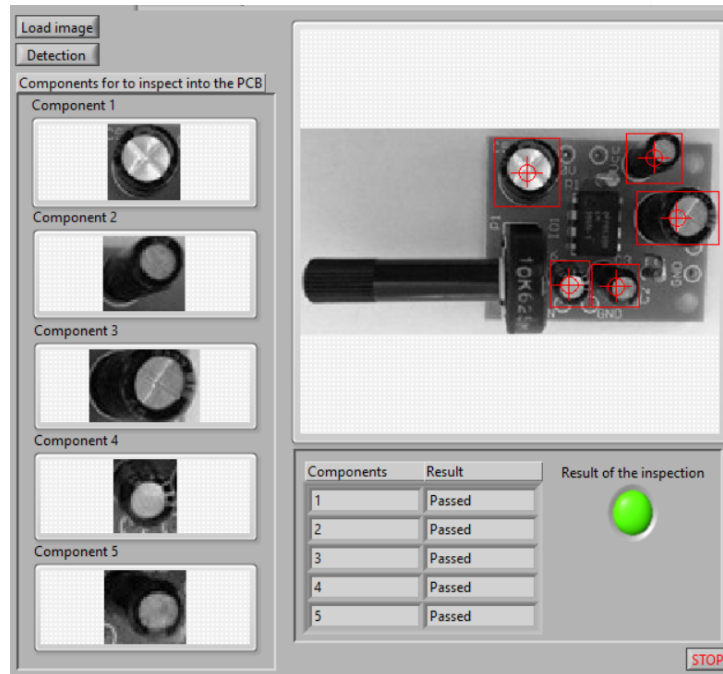


Figure 6 - Example of an optical inspection.

## 1.2. Cameras usage on an industrial vision system

During the process of obtaining images, the use of cameras plays a key role in the extraction of information, since it is a device capable of taking visual representations of situations or objects, which will then be processed to extract certain necessary information depending on the type of application, for example, color extraction. Currently, there are normal cameras, which oversee simply capturing images unlike a new type of cameras that allows performing pattern recognition or image analysis, called "smart cameras" (see Figure 7), a group of devices capable of delivering a high performance like human eyes and brain using artificial intelligence. [6]

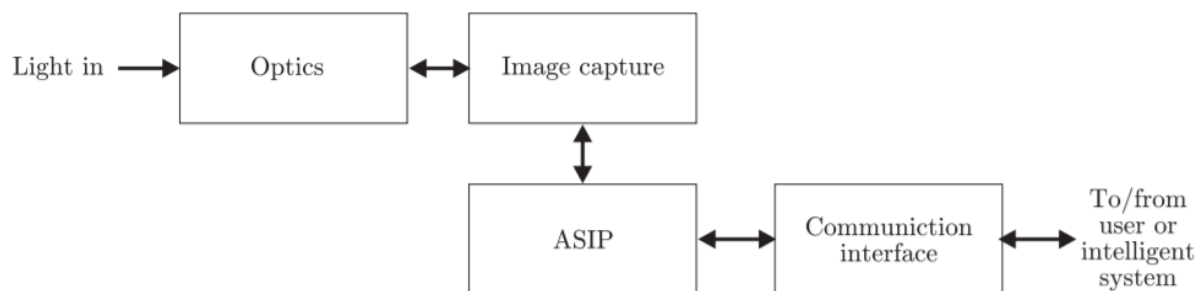


Figure 7 - The structure of a typical smart camera. ASIP: Application-Specific Information Processing. [6]

### 1.2.1. Types of sensors implemented on cameras

Today, the cameras, whether industrial or consumer, compact or reflex (camera in which the photographer can see the image through the optical viewfinder) are manufactured based on Metal-Oxide-Semiconductor

sensors (MOS) which are distributed in the form of a matrix to capture the necessary amount of light and create electrical charges, which will be stored in the pixels.

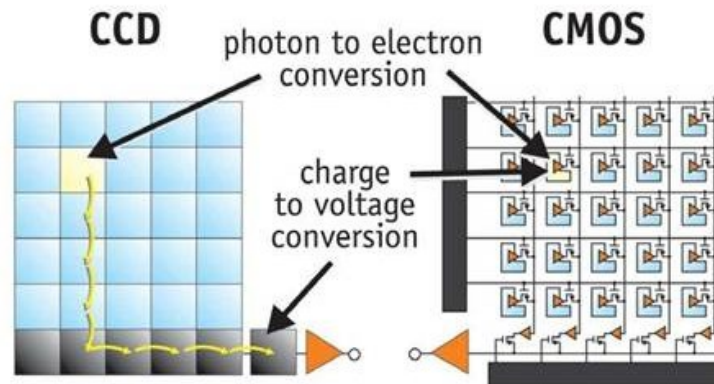


Figure 8 - Light to voltage conversion difference between CCD and CMOS sensors. [7]

These types of sensors are classified as:

- **CCD sensor (Charge-coupled device sensor)**

The CDD sensor receives the charges in voltages to send them as an analog signal that will be digitized, in such a way that the values are read in pixels and then converted in an analog-digital way into data, due to this the camera needs a device that can read information, which causes the device to be larger. This sensor has an advantage when it comes to tolerating light due to the saturation of pixels and the threshold by which they do not capture a signal in the sound aspect is higher because it uses an external chip to optimize the function, unlike CMOS which performs the process photon to charge internally on each pixel and due to the photo-diodes do not have much space to collect light, between these two sensors when they are subjected to the same level of excitation the CCD sensor has better behavior as it has a uniform response matrix (see Figure 8).

- **CMOS sensor (Complementary metal-oxide-semiconductor)**

These sensors are more compact, the converter photon to charge that each cell carries allow the pixels not to need another extra device for their operation, an advantage of being more compact compared to CCD sensors and offer better quality both in the performance of the final product of the device since it has signal amplifiers that have their cells, which makes them more sensitive to light, having a lower power consumption (see Figure 8). A common disadvantage that CCD sensors have compared to CMOS is that they are usually affected by blooming, this effect is due to the light many pixels tend to saturate and affect the pixels around them.



## 1.2.2. Classification of smart cameras implemented on artificial vision

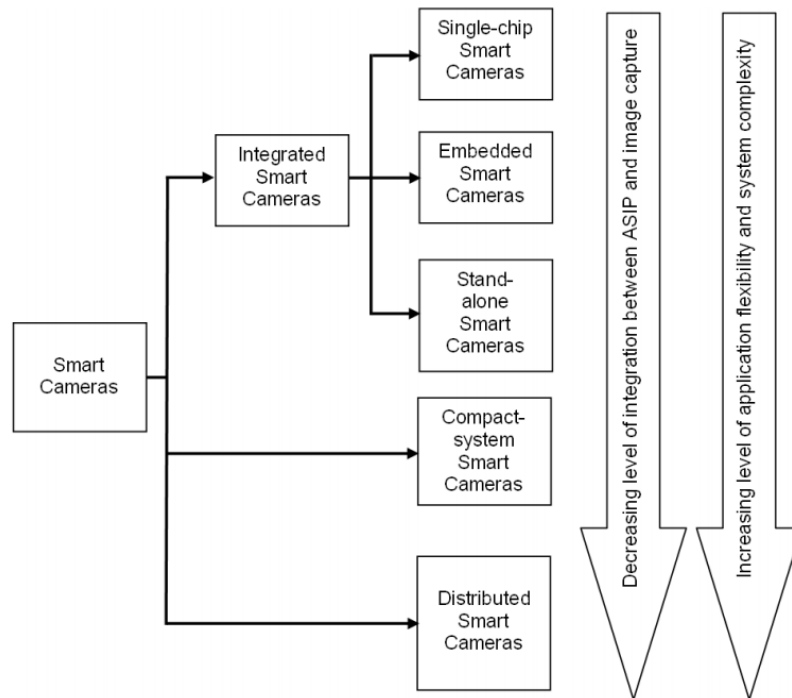


Figure 9 - Classification of smart cameras implemented on artificial vision. [6]

The selection of a suitable camera depending on the type of application, during the design of an image processing system, generates great advantages in the information extraction phase, such as ease in handling high-speed signals and image processing tasks due to the implementation of high-performance microprocessors (e.g. FPGA, DSP). Leading to the system is autonomous and avoiding error when the signal is capturing or losing the quality of the image.

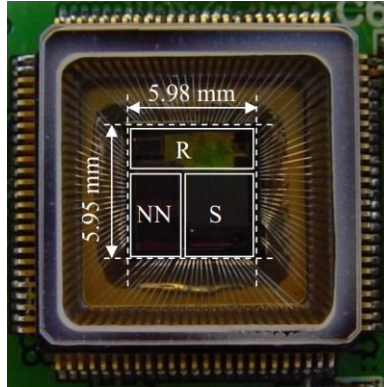


Figure 10 - Example of Smart cameras: Sony XCI-SX1 smart camera for machine vision applications (left photo); Intellio ILC-210 smart camera for security and surveillance applications (right photo). [6]

These types of cameras are classified according to certain characteristics that differentiate them from conventional cameras (see Figure 9), for example, the structure of the ASIP block (a block made up of a powerful integrated microprocessor).

- **Single-chip smart cameras**

Single-chip smart camera is the type of camera that contains the application-specific information processing module (ASIP) on the same chip as the image sensor (see Figure 11). Due to this design, this type of camera has lower power consumption, high efficiency, and small size. given that the device does not occupy a big space, it is used on toys or pervasive information sensors. [6]



*Figure 11 - Example of a Single-chip smart camera (VISoc Chip: NN-vision/neural processor, S-sensor, R-RISC processor). [8]*

- **Embedded smart cameras**

When the camera is implemented on the design of another device and the functionality of the ASIP module comes from the embedded device, it is called an embedded smart camera. Usually, this type of cameras are used on fingerprint readers, mobile phone, etc. [6]

- **Stand-alone smart cameras**

This type of camera is like normal cameras implemented in a CCTV, unlike the ASIP functionality consists of intelligent algorithms executing on the embedded processors. Due to this characteristic, the stand-alone smart cameras are part of industrial machine vision applications or human-computer interfaces (an example of stand-alone smart cameras see Figure 10). [6]

- **Compact-system smart cameras**

Unlike the integrated smart cameras, this type of camera has the application-specific information processing module (ASIP) separate from an embedded processor nearby. Usually, the compact-system smart camera is in charge just to perform the image acquisition and some pre-processing functions, for example, to extract characteristics from the image but the rest of the ASIP functionality is performed by an external unit.

- **Distributed smart cameras**

The distribute smart cameras consist of the implementation of different cameras interconnects between them (see Figure 12), forming a distributed system (network of distributed smart cameras) where the

images acquired are sent to the ASIP module, which has the functionality to perform a specific image processing application. [9]

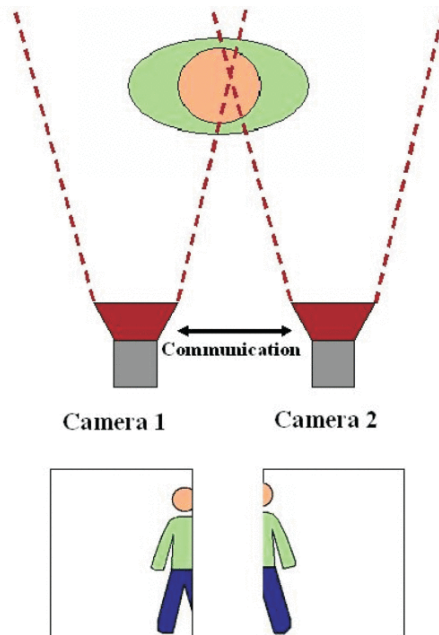


*Figure 12 - Example of distributed smart camera's structure (subject captured by a distributed smart camera system) [9]*

### **1.2.3. Camera lenses and filters**

The lens is the component in charge of directing light rays towards the sensor to obtain a clear image. The implementation of the lens to the camera allows adjusting the focal length, focus, or aperture of the diaphragm. Currently, there are several types of lenses, such as:

- **Normal Lens**

Normal lenses are the lenses that most closely resemble human vision, they are one of the simplest lenses because it is built with fewer lenses. normal lenses have a focal length of 50mm, offer good quality and brightness when taking images.

- **Wide-angle Lens**

Wide-angle lenses, unlike normal lenses, have a shorter focal length (between 18 and 35mm) so it allows taking panoramic photos.

- **Telephoto Lens**

Telephoto lenses are those that allow you to photograph distant objects because their focal length is much greater than that of normal lenses (between 135 to 300+mm).

But during the taking of images, certain external sources can influence and distort the information that will later be analyzed, for example, ambient light. To correct this problem, certain filters with a specific function can be adapted to the lenses.

- **UV filter**

The UV filters are responsible for preventing ultraviolet light from reaching the camera's sensor.

- **Polarizing filter**

The polarization filters are those that allow taking photos of metal objects, avoiding the glare of light.

- **Neutral density filter**

Neutral density filters are those capable of reducing the amount of light that reaches the sensor when taking a photo.

### 1.2.4. Camera interface

Not only is it necessary to specify the type of camera, but it is also crucial to clarify the components that are used to work with the camera, which facilitates self-control, good image acquisition quality, and excellent communication with the complete system (see Figure 13).

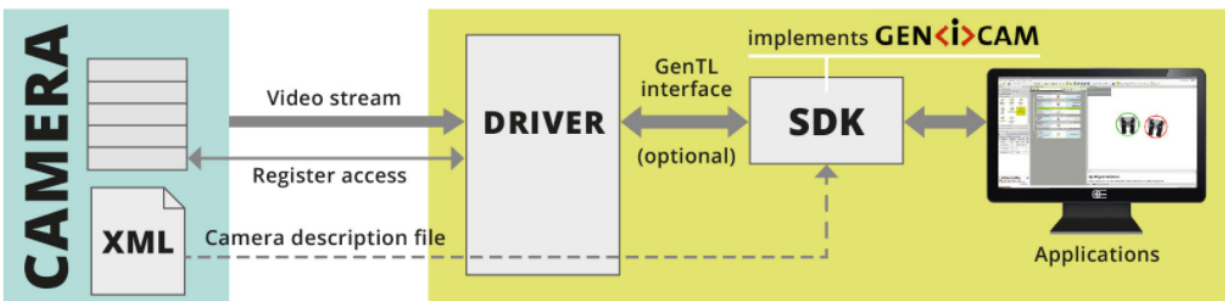


Figure 13 - Generic interface of a camera. [10]

- **Controller**

A device in charge to perform the communication between the camera to the computer.

- **Software development kit (SDK)**

The SDK is the software development tool that makes it easy to control the camera from the application programming interface (API). Typically, this development toolkit contains code (code that can be written in a specific programming language, for example, C, C ++, etc.), technical papers, or other notes that facilitate good functionality and avoid error during implementation.

- **Communication interfaces**

The communication interface is the cable communication protocol that allows images to be obtained from the camera and transmitted to the device (for example a computer) where the user application is located. but to define the type of communication protocol it is necessary to consider the following factors

1. Data reception/transmission rate (bandwidth).
2. Specifications of the wire (type, maximum cable length, and wireless range).
3. Communication latencies and robustness.
4. Compatibility issues and software drivers.

*Table 2 - Wired communication protocols. [6]*

<b>Protocol</b>	<b>Theoretical bandwidth in bits per second (bit/s)</b>
USB 2.0 Hi - speed	480 Mbit/s
FireWire or IEEE 1394a/b	400/800 Mbit/s
Camera Link	2.04, 4.08 or 5.44 Gbit/s
Fast Ethernet	100 Mbit/s
GigE Vision (Gigabit Ethernet)	1 Gbit/s
CoaXPress (CXP) 2.0	12.5 Gbit/s
USB 3.0	5 Gbit/s

### **1.3. Illumination using an industrial vision system**

As shown in Figure 1, lighting is a fundamental part of obtaining information during image processing. The adequate selection of the lighting component depending on the application to be made, guarantees no loss of information, a definition in the details of the object to be inspected (maximizing or minimizing the contrast), among other advantages.

For to select the most appropriate light is necessary to consider:

- The geometry of the light.
- Light source type (see Figure 15).
- Wavelength.
- Object shape.
- Environment considerations.

#### **1.3.1. Type of light concerning wavelength**

Light can be classified according to wavelength, in other words, light is electromagnetic radiation that contains a fraction of the electromagnetic spectrum (see Figure 14).

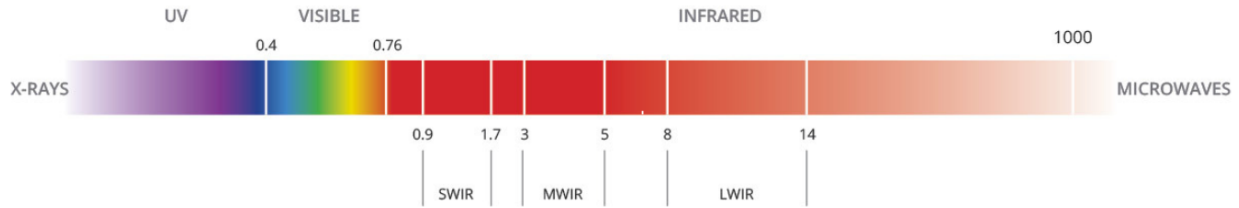


Figure 14 – Part of the electromagnetic spectrum. [11]

- Quasi-monochromatic contains just a single color, which means that it has a narrow wavelength band.
- White light contains all colors, which means that it is distributed over all visible electromagnetic spectrum.
- Infrared (IR), light with a wavelength range goes from about 0.7 to 1000 micrometers.
- Ultraviolet (UV), light with a wavelength nearly to 10 nm ( $10 \times 10^{-9}$  m) and 400 nm ( $400 \times 10^{-9}$  m).

### 1.3.2. Light sources

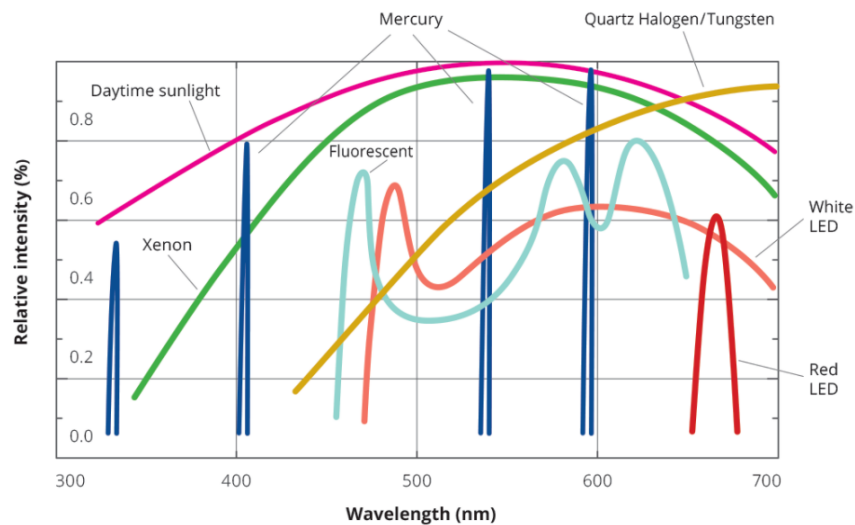


Figure 15 - Emission spectra of different light sources. [12]

#### - Incandescent lamps

They are the type of lamps that produce light when an electric current circulates through the filament (metallic conductor) that is transformed into heat, a method called the joule effect (See Figure 16). [13]

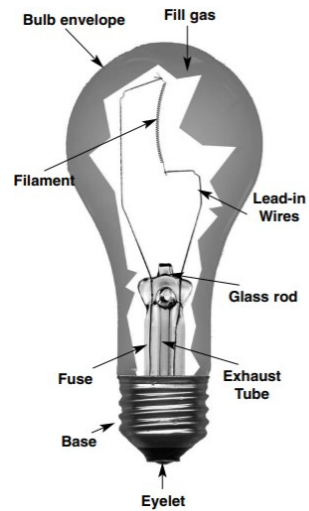


Figure 16 - Structure of incandescent lamps. [13]

- **Fluorescent lamps**

Fluorescent lamps are a type of fluorescent tube composed of mercury liquid (See Figure 15) and another substance, when they receive ultraviolet radiation, they produce visible light (See Figure 17). [12]

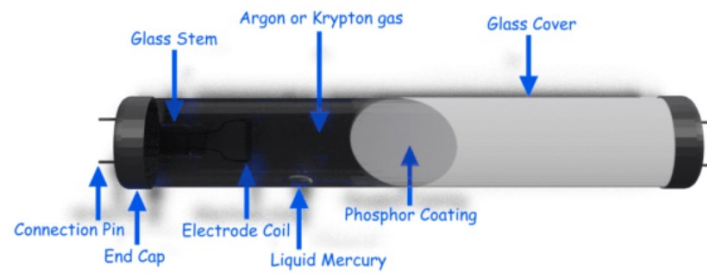
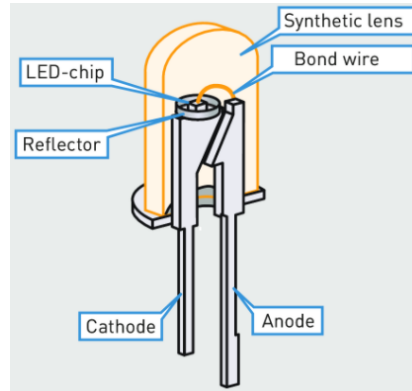


Figure 17 - Example of a structure of a fluorescent lamp. [14]

- **LED lights**

The light-emitting diode is a semiconductor composed of two terminals, one positive and one negative (anode and cathode) connected to a PN junction diode. when a voltage is applied between the two terminals, the energy is released in the form of photons (electroluminescence effect), therefore the diode emitted a quasi-monochromatic light (See Figure 18). [15]



*Figure 18 - Structure of a light-emitting diode. [15]*



## 2. Description of the development environments and development technologies used in the visual inspection of industrial product

To develop applications for image processing, there are currently different types of programming languages, which contain libraries of functions or environments developed for handling images (An example, see Figure 19). Some of the environments used in computer vision are:

- LabVIEW
- Open CV
- Visual Applets
- MATLAB

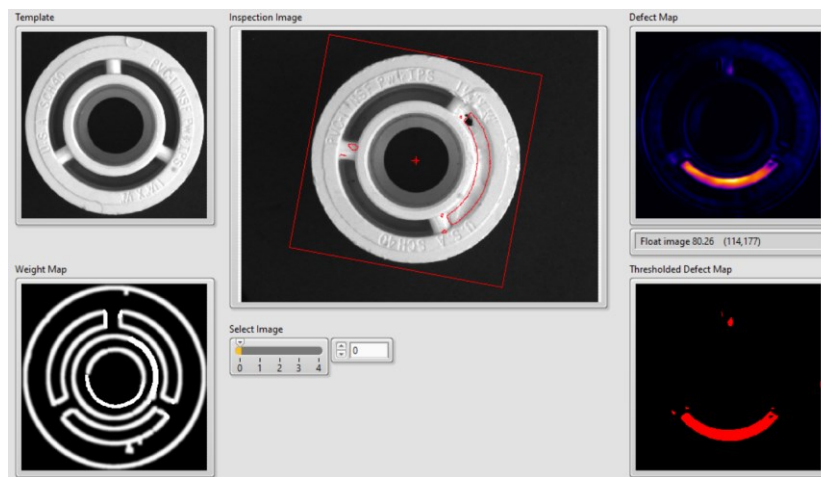


Figure 19 - Object inspection example developed in LabVIEW.

This chapter focuses on the description of the environment and the functions it contains for the processing of images for the solution of the proposed problem, in this case, LabVIEW was used as a programming language to perform the inspection of industrial products through 3D reconstruction using the model photometric stereo.

LabVIEW is a programming language composed of blocks, called Virtual Instruments (VIs) with specific functions (See Figure 20), where the programmer can connect these blocks to develop a block diagram that represents the operation of a certain process or program (See figure 20)

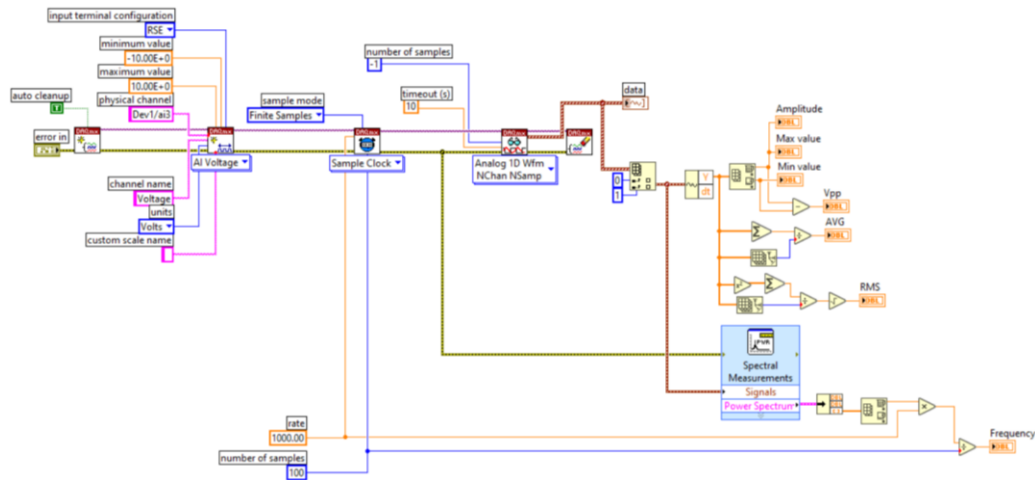


Figure 20 - Example of a block diagram created in LabVIEW.

Currently, LabVIEW contains libraries capable of analyzing, processing images, and implementing machine vision to carry out a specific application. For example, locate objects to inspect.

- **Vision Acquisition SW NI-IMAQ**

Software that allows you to acquire, save and display images from different types of cameras with different communication protocols. This software also allows modifications to be made to the configuration of the camera to be used, for example, changing the exposure time or the size of the image, among other parameters.

- **Vision development module**

A LabVIEW module (function library) that contains functions that can be implemented when carrying out vision machine applications (See Table 3).

Table 3 – Some function blocks implemented on vision applications. [16]

Getting measurement – Ready images	Grayscale and color measurement	Blob analysis	Machine vision	Calibration
Set up an imaging system	Define regions of interest	Correct image distortion	Locate objects to inspect	Perspective and nonlinear distortion calibration
Calibrate imaging system	Measure grayscale statistics	Create binary image	Set search areas	Simple calibration
Create image	Measure color statistics	Improve the binary image	Find measurement points	Save calibration information
Read an image	Learning color information	Make particle measurements	Convert pixel coordinates to Real-World coordinates	Attach calibration information
Display an image		Convert pixel coordinates to Real-World coordinates	Make measurements	
Attach calibration information			Display results	
Analyze an image				
Improve image functions (Filters, FFT, Grayscale morphology, etc.)				

### 3. Theoretical analysis of 3D reconstruction with Photometric Stereo approach

#### 3.1. Lighting

Currently, it is known that an image is a representation of an object or space taken by a camera, the human eye, or another type of sensor capable of processing reflected light. But to carry out the process of generating an image through reflected light it is necessary to implement a light source, for example, ambient light (The sun). A light source that falls on the surface and helps determine the brightness of each point on the surface based on the characteristics of the surface (see Figure 21). [17]

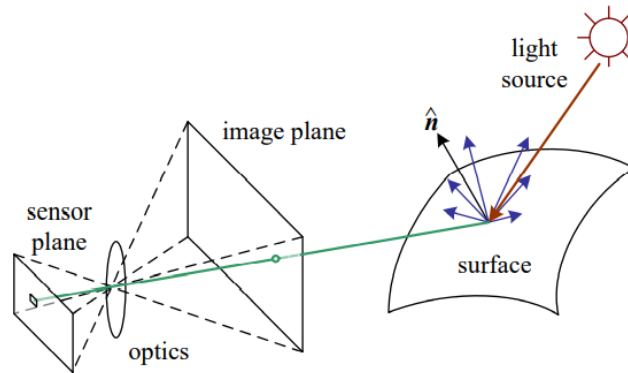


Figure 21 - Model of image formation. [17]

The light source can be divided according to its origin and the behavior when the light is emitted as:

- **Point light source**

The point light source is when the light comes from a specific location and the light emission is the same in all directions (see Figure 22).

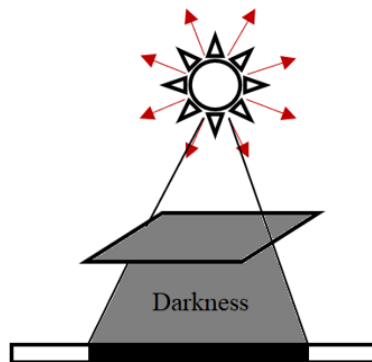


Figure 22 - Description of a point light source.

The intensity of the light decreases depending on the inverse square law (Eq. 1), the rule that describes that the intensity reduces with a distance (see Figure 23). [18]

$$I = \frac{S}{2\pi r^2} \left[ \frac{W}{m^2} \right] \quad \text{Eq. 1}$$

Where

- $I \left[ \frac{W}{m^2} \right]$  is defined as the intensity at the surface of the sphere, which means the amount of light obtained per area.
- $S [W]$  represents the source strength.
- $r [m]$  is the radius.

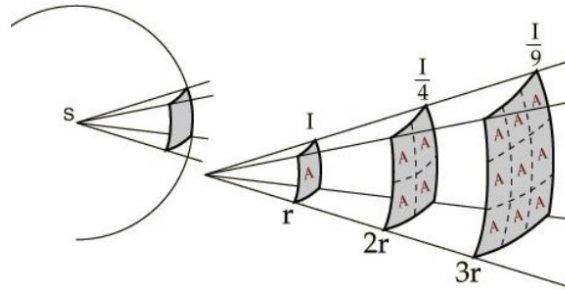


Figure 23 - Description of the inverse square law. [18]

▪ **Area light source**

The light originates from a rectangular area and the light is emitted through the surface area (see Figure 24). [17]

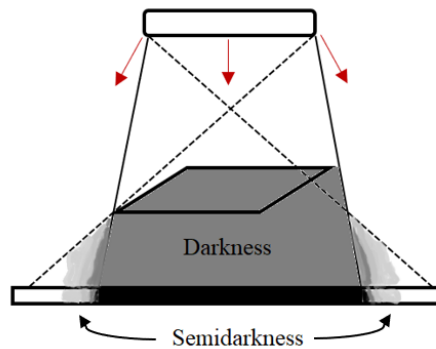


Figure 24 - Description of an area light source.

### 3.2. Phenomena of reflectance

During the imaging process, it is not only necessary to know what the light source is like, but it is also important to identify the characteristics of the surface, especially the reflectivity of the material. A property that defines the amount of light that is reflected from the surface (see Figure 25) or objects towards the sensor (Device implemented for the detection of reflected light). [19]

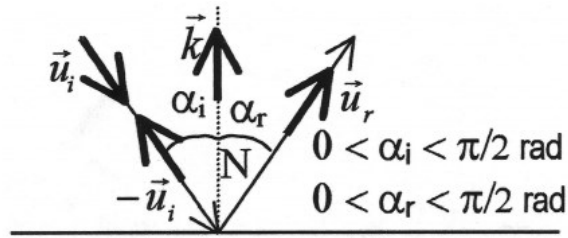


Figure 25 - Diagram of the law of reflection. [20]

### 3.2.1. Analysis of a surface reflectance

But this reflectivity property can be influenced by the type of reflection from the surface, how smooth or rough the surface is (see Figure 26)

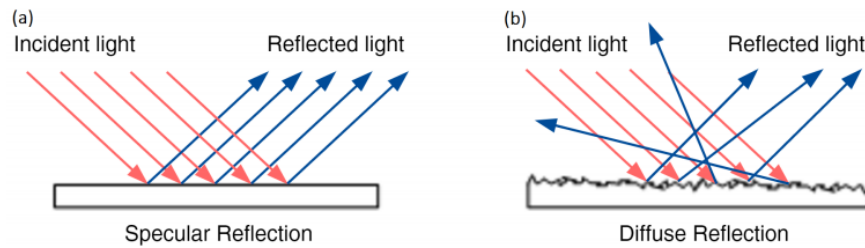


Figure 26 - Specular and diffuse reflection from an object surface. [1]

- **Specular reflection**

The specular reflection is mostly a phenomenon that is produced on smooth surfaces when the incident lights ( $\hat{v}_i$ ) are reflected ( $\hat{s}_i$ ) to 180 degrees around the normal surface (see Figure 27). [17]

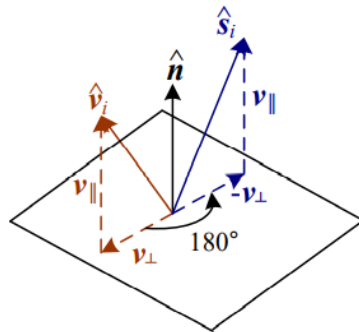


Figure 27 - Specular reflection. [17]

- **Diffuse reflection**

Unlike the specular reflection, the diffuse reflection is generated on rough surfaces and the incident lights are scattered at different angles from the surface (see Figure 28). [1]

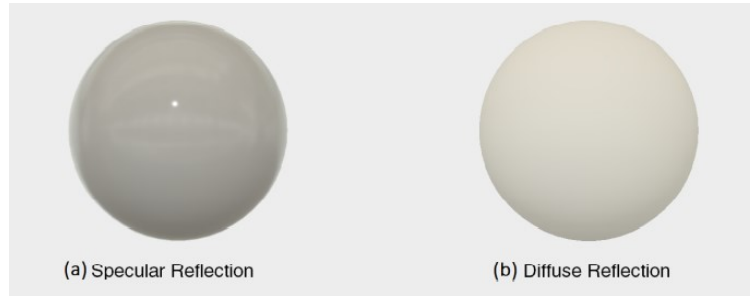


Figure 28 - Example of specular and diffuse reflection under the same light source and same spherical object. [1]

### 3.2.2. Bidirectional reflectance distribution function

The diffuse reflection follows the scattering model called Bidirectional reflectance distribution function (BRDF), a model that determines the amount of each reflected light ( $\hat{v}_r$ ) depending on the incident light ( $\hat{v}_i$ ) (see Figure 29). [17]

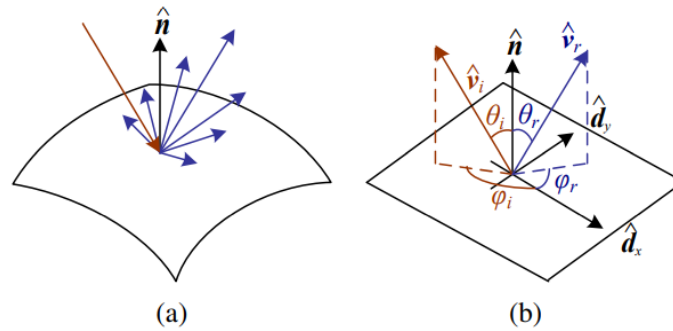


Figure 29 - (a) Example of light scatters, (b) The bidirectional reflectance distribution function. [17]

The BRDF could be represented by the equation depending on the angles of the incident and reflected light respecting the surface (Eq. 2). [17]

$$f_r(\theta_i, \phi_i, \theta_r, \phi_r; \lambda) \quad [sr^{-1}] \quad \text{Eq. 2}$$

This distribution function has the property of Helmholtz reciprocity, which means that it is possible to change the roles between the incident and reflected vector without affecting the bidirectional distribution function. Also, the reflected light could not be negative for any direction. [3]

Besides, when the material has the same property for each point of view, commonly called Isotropic materials, the bidirectional reflectance distribution function could be simplified using the vectors of reflected light ( $\hat{v}_r$ ), incident light ( $\hat{v}_i$ ) and normal vector ( $\hat{n}$ ) (Eq. 3).

$$f_r(\hat{v}_i, \hat{v}_r, \hat{n}; \lambda) \quad [sr^{-1}] \quad \text{Eq. 3}$$

This new representation gives the possibility to calculate the amount of reflected light depending on the BRDF (Eq. 3), the amount of incident light through the material, and a new factor called the foreshortening factor (Eq. 4). [17]

$$L_r(\hat{v}_r; \lambda) = \int L_i(\hat{v}_i; \lambda) f_r(\hat{v}_i, \hat{v}_r, \hat{n}; \lambda) \cos^+ \theta_i d\hat{v}_i \quad [lx] \quad \text{Eq. 4}$$

Where this foreshortening factor is defined as

$$\cos^+ \theta_i = \max(0, \theta_i) \quad \text{Eq. 5}$$

A factor that relates to the amount of light reflected regarding the direction of the incident light ( $\hat{v}_i$ ) to the normal surface ( $\hat{n}$ ) as  $\hat{v}_i \cdot \hat{n}$ , to help perceive the depth of the object (see Figure 30). [17]

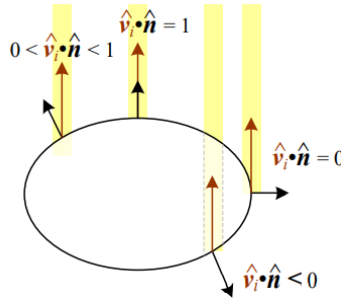


Figure 30 - The reduction of reflected light caused by the foreshortening factor varies on, the cosine of the angle between the incident light direction and the normal surface. [17]

### 3.3. Lambertian reflectance model

The Lambertian reflectance model is the easiest type of bidirectional reflectance distribution model (see Figure 31) and it occurs when the reflected light spreads uniformly in all directions, giving the possibility to the sensor (for example, a camera) to acquire an image of the object surface. [1]

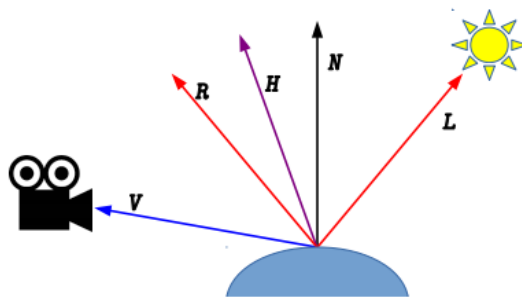


Figure 31 - Vectors for modeling BRDFs. [3]



The amount of light reflected from each point that made up the image varies with the angle according to Lambert's law, which specifies that the intensity of the reflected light is proportional to the cosine between the incident light with the normal surface (Eq. 6). [3]

$$i_d(u, v) \propto \max(\bar{N}(u, v) \cdot \bar{L}(u, v), 0) \quad \text{Eq. 6}$$

As the Lambertian model is frequently used to modeled diffuse reflection (see Figure 32), then the intensity of reflection could be calculated as the following equation (Eq. 7).

$$I_p = \sum_{i=1}^k \rho_{i,p}^t [f_i(n_p, L_p, v)] \quad \text{Eq. 7}$$

Where the equation is composed by:

- The intensity ( $I_p$ ) for a specific point P
- The reflection coefficient ( $\rho^t$ ) through the surface
- The reflectance map ( $f_i$ ) as a function of viewing direction  $v$
- The normal surface ( $n_p$ )
- The incident brightness field ( $L_p$ )
- The value of a linear combination of  $k$  material

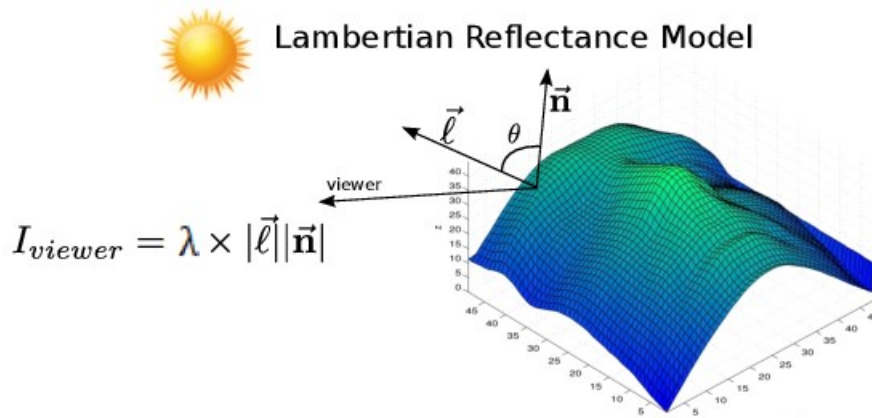


Figure 32 - Lambertian reflection model. [21]

Simplifying the process to obtain the image of the object surface, the reflectance characteristic is usually modeled as a first-order approximation, giving, as a result, the following equation (Eq. 8). [1]

$$I(\vec{v}) = \lambda(\vec{v}) \vec{n}(\vec{v}) \cdot \vec{l} \quad \text{Eq. 8}$$

Where the equation is composed by:

- The image  $I(\vec{v})$

- The surface Albedo  $\lambda(\vec{\tau})$
- The normal surface  $\vec{n}(\vec{\tau})$
- The light source  $\vec{l}$

### 3.3.1. Surface Albedo

The surface Albedo is a characteristic that represents the amount of the incident radiation that is reflected through the object surface (see Figure 33). [22]

$$\alpha_\lambda = \frac{F_\lambda^+}{F_\lambda^-} \quad \text{Eq. 9}$$

Eq. 9 describes that the spectral Albedo depending on the wavelength illumination ( $\alpha_\lambda$ ) is the ratio between the flux of light incident ( $F_\lambda^-$ ) on the object surface with the flux of light reflected through the surface ( $F_\lambda^+$ ). [22]

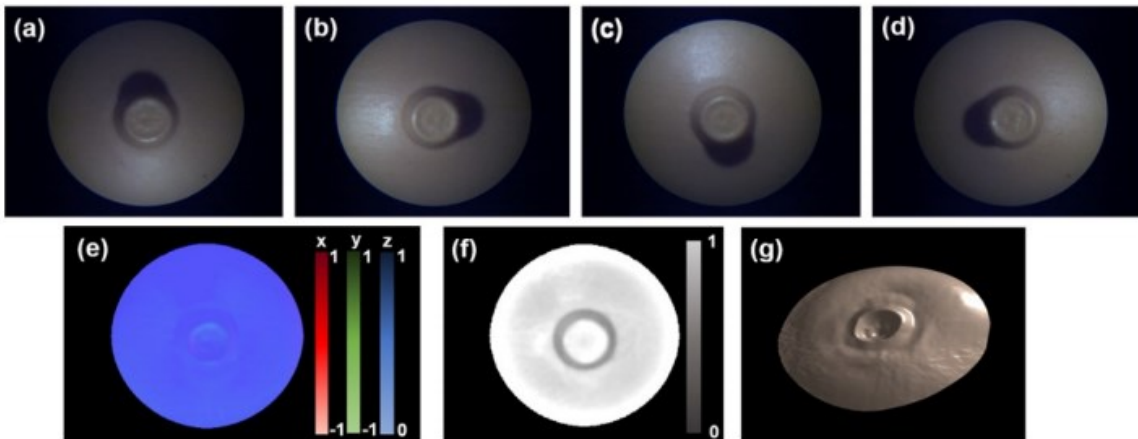


Figure 33 - (a–d) Images acquired at different illumination directions, (e) Surface normal image, (f) albedo map, and (g) Reconstructed 3D image. [23]

### 3.3.2. Normal surface

The normal surface is composed of each perpendicular vector of every point to the tangent plane of the object surface (see Figure 34).

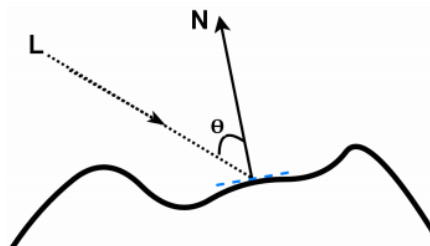


Figure 34 - Explanation of how the normal vector (N) is formed from the incident light (L). [1]

### 3.3.3. Depth map

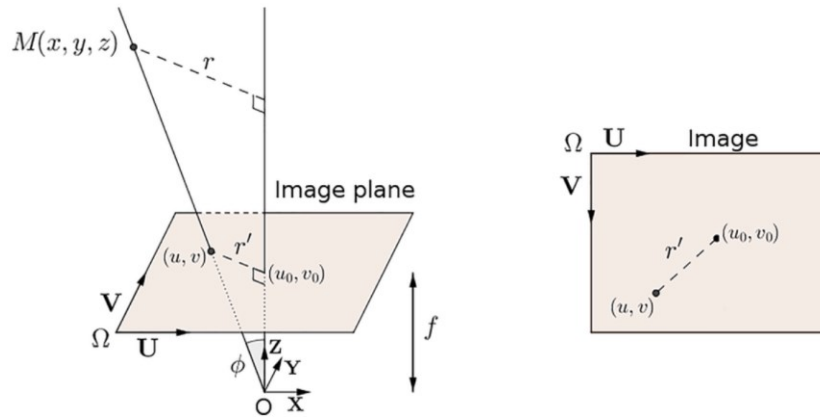


Figure 35 - Relationship between Cartesian coordinates and image coordinates. [24]

The object to be 3D reconstructed is parametrized by a set of three-dimension points, as the following equation (Eq. 10).

$$[x(u, v), y(u, v), z(u, v)] \quad \text{Eq. 10}$$

Where the  $x$  and  $y$  coordinates are defined using the image plane coordinates  $u$  and  $v$  (presuming orthographic camera viewing – see Figure 35). [3]

$$x(u, v) = u \quad \text{Eq. 11}$$

$$y(u, v) = v \quad \text{Eq. 12}$$

Using the results of the normal surface ( $N(u, v)$ ), it is possible to calculate an image, that contains information regarding the distance from the sensor, in this case, a camera to the object surface, image mostly called depth surface ( $z(u, v)$ ) (see Figure 36).

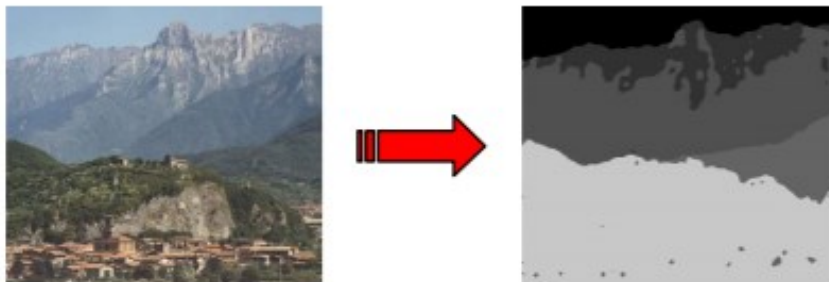


Figure 36 - Example of a depth map. [25]

Assuming that the depth map is differentiable, and the normal surface contains the integrability constraint, it is obtained the following equation (Eq. 13). [3]

$$N(u, v) \propto \left[ \frac{\partial z(u, v)}{\partial u}, \frac{\partial z(u, v)}{\partial v}, -1 \right]^T \quad \text{Eq. 13}$$

But avoiding the integration process to obtain the depth map, it is possible to implement the Eikonal equation (Eq. 14). [3]

$$\|\nabla t(u, v)\| = \frac{1}{f(u, v)} \quad \text{Eq. 14}$$

And introducing auxiliary variables

$$p = \frac{\partial z}{\partial u} \quad \text{Eq. 15}$$

$$q = \frac{\partial z}{\partial v} \quad \text{Eq. 16}$$

Finally, the calculation of the depth map (See an example in Figure 36) is carried out as in the following equation (Eq. 17).

$$\nabla^2 z(u, v) = \frac{\partial p}{\partial u} + \frac{\partial q}{\partial v} \quad \text{Eq. 17}$$

### 3.4. Shape from shading procedure

The shape from shading (SFS) procedure is a method that consists of making a 3D reconstruction from a single image. Using the geometric characteristic of the object surface and the parameters from the incident light source, to calculate the intensity of each 2D point, assuming a Lambertian reflectance model.

Using the reflectance surface ( $R(p, q)$ ) to describe a relation respecting the surface gradient (first partial derivatives of  $z$  concerning the coordinates  $x$  and  $y$ ), is obtained the following equation (Eq. 18). [1]

$$(p, q) = \left( \frac{\partial z}{\partial x}, \frac{\partial z}{\partial y} \right) \quad \text{Eq. 18}$$

But when the brightness map of the object surface is known ( $I(x, y)$ ), It limits the chance of what the surface orientation at a particular point of the object could be and the relation between the reflectance surface with the brightness map is giving by Eq. 19. [26]

$$R(p(x, y), q(x, y)) = I(x, y) \quad \text{Eq. 19}$$

### 3.5. Photometric stereo

Photometric stereo is a methodology that allows obtaining the appearance of an object by analyzing the item under different illumination directions (see Figure 37). The process consists of taking different pictures from the object with a camera by different changes of illumination directions, giving the possibility to estimate the depth and surface of the object. [27]

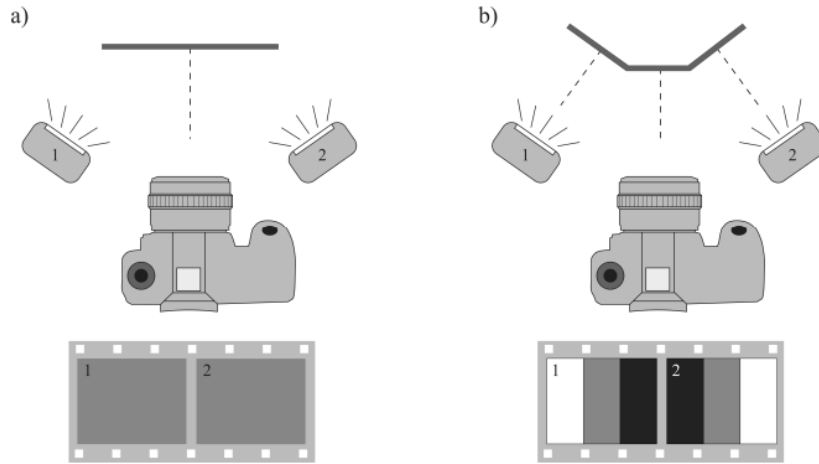


Figure 37 - Principle of photometric stereo. a) Intensity of the object when the surface is flat and normal to the camera. b) Intensity of an uneven object [1].

As previously said that Photometric Stereo requires a change in lighting directions, for this needs a controller in charge of that function and that the object and camera are fixed during the process of obtaining the images (see Figure 38). [1]

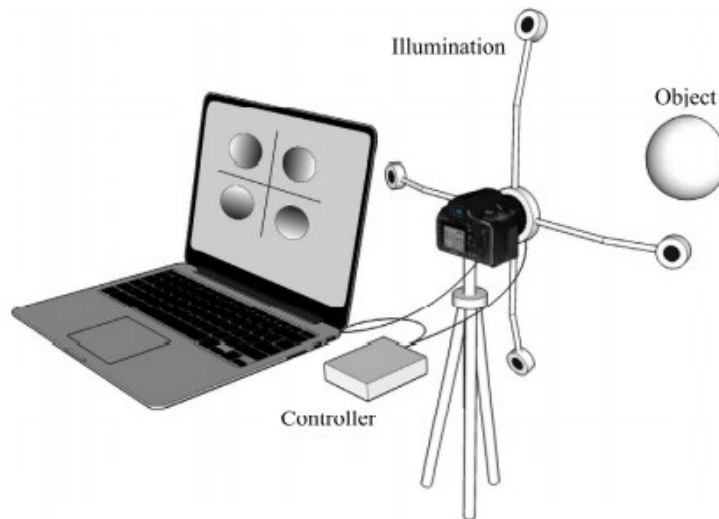


Figure 38 - Example of schematics for Photometric stereo model. [27]

### 3.5.1. Mathematical description

To develop the 3D reconstruction, the minimum number of pictures to implement is three and to analyze them using (Eq. 8), it is necessary to implement algebra linear.

$$\begin{bmatrix} I_1 \\ I_2 \\ I_3 \\ I_4 \end{bmatrix} = \lambda \cdot \begin{bmatrix} l_{x_1} & l_{y_1} & l_{z_1} \\ l_{x_2} & l_{y_2} & l_{z_2} \\ l_{x_3} & l_{y_3} & l_{z_3} \\ l_{x_4} & l_{y_4} & l_{z_4} \end{bmatrix} \cdot \begin{bmatrix} n_x \\ n_y \\ n_z \end{bmatrix} \quad \text{Eq. 20}$$

Where the equation (Eq. 20) is composed by:

- The image intensity ( $I_n(x, y)$ )
- The surface Albedo ( $\lambda(\vec{l})$ )
- The unit illumination vector ( $L_n = (l_x, l_y, l_z)_n$ )
- The normal surface (N)

The implementation of equation 20 leads to having certain conditions regarding the illuminance vectors ( $L_1, L_2, L_3, L_4$  – see Figure 39) and the  $L$  matrix.

1. The illuminance vectors ( $L_1, L_2, L_3, L_4$ ) should be non-coplanar, which means that they do not intersect between them (no common plane). [1]
2. The matrix  $L$  should be a non-singular matrix, which means that is possible to calculate the inverse matrix from the regular matrix. [1]

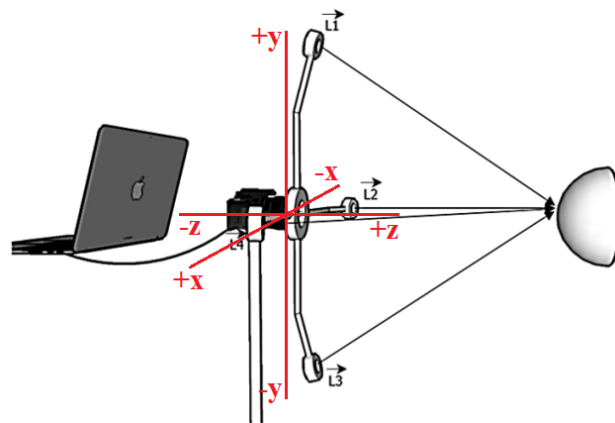


Figure 39 - Location of the lighting system (Necessary parameter to build the lighting vector -  $L_n$ ). [1]

When those conditions are fulfilled, the normal surface is possible to calculate using the following equation (Eq. 21).

$$N = (1/\lambda)L^{-1} \cdot I \quad \text{Eq. 21}$$

## 4. Design of an inspection of industrial product

As the main objective of the project is to design an inspection system capable of taking images of an object under different changes of lighting directions, to perform a 3D reconstruction of the surface (see Figure 40) and thus be able to analyze it and determine if the product contains (or not) surface defects such as cracks or problems in the geometry of the object.



Figure 40 - Example of 3D reconstruction result using photometric stereo.

### 4.1. Requirements for optical inspection

But some requirements must be considered when selecting the appropriate hardware and software to design the image processing system to be implemented (see Table 4):

- The selection of an adequate camera requires knowing the size, geometry, how big are the recognizable features of the surface, and other characteristics associated with the test object. Information that helps to identify for example the resolution of the camera, the type of lens, etc.
- To make visible the defects and details of the object, it is necessary to select a good illumination system, that will help to contrast with the environment. To select the type of lighting to implement, the type of surface, shape, type of material, and color of the object must be considered.
- The software tool in charge of algorithms to make the image processing, it should be chosen depending on the type of activity (e.g. present checks, object search, etc.).

Table 4 - Some criteria to design an image processing model.

Parameters necessary to design an optical inspection model				
Test object	Camera & sensor	Lens	Illumination	Machine vision system
Size	Resolution	Focal length	Form factor	Software algorithms
Geometry	Sensor size	Resolution	Working distance	Speed
Surface	Mono / color	Image circle diameter	Color light	Interfaces
Material	Sensor type (CCD / CMOS)		Direct / diffuse light	
Color	Interface		Intensity	
			Alignment	

## 4.2. Description of the solution

When all the specifications are defined and the type of inspection is selected, in this case, the stereo photometric approach was implemented to perform a 3D reconstruction. It is necessary to define the different activities that are carried out in the information measurement system (see Figure 41).

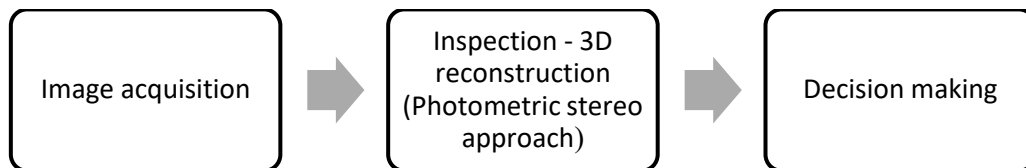
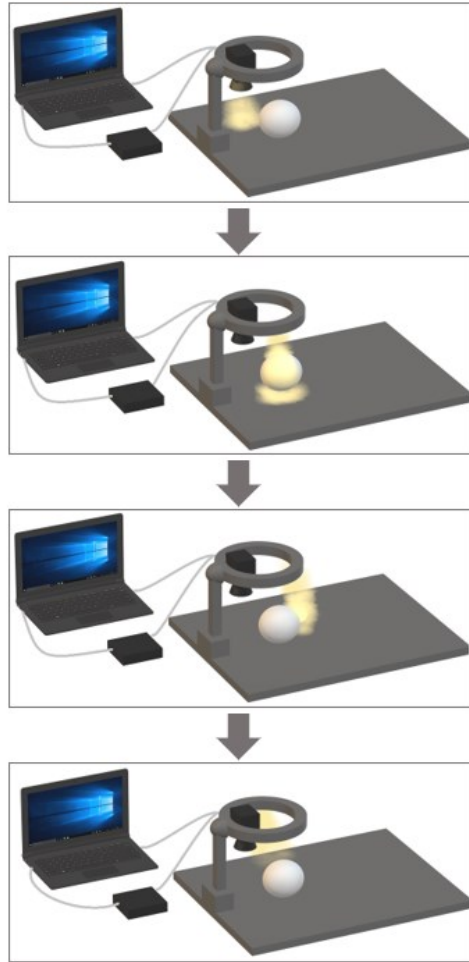


Figure 41 – Main blocks for the project solution.

### - Image acquisition

The image acquisition phase is responsible for taking the images and preparing them for the reconstruction process. As the model chosen for the reconstruction was photometric stereo, it is necessary to take at least 3 images with different lighting directions. For this case, 4 images will be taken with light directions up, down, left, and right (see Figure 42).





*Figure 42 - Procedure for image acquisition.*

- **Inspection 3D reconstruction (Photometric stereo approach)**

After the images are obtained, the 3D reconstruction is carried out, a procedure that consists of extracting the normal surface and the Albedo surface depending on the positions of the lighting direction, when these two surfaces are calculated, we proceed to calculate the gradients, variable that will allow the computation of the depth map (see Figure 43).

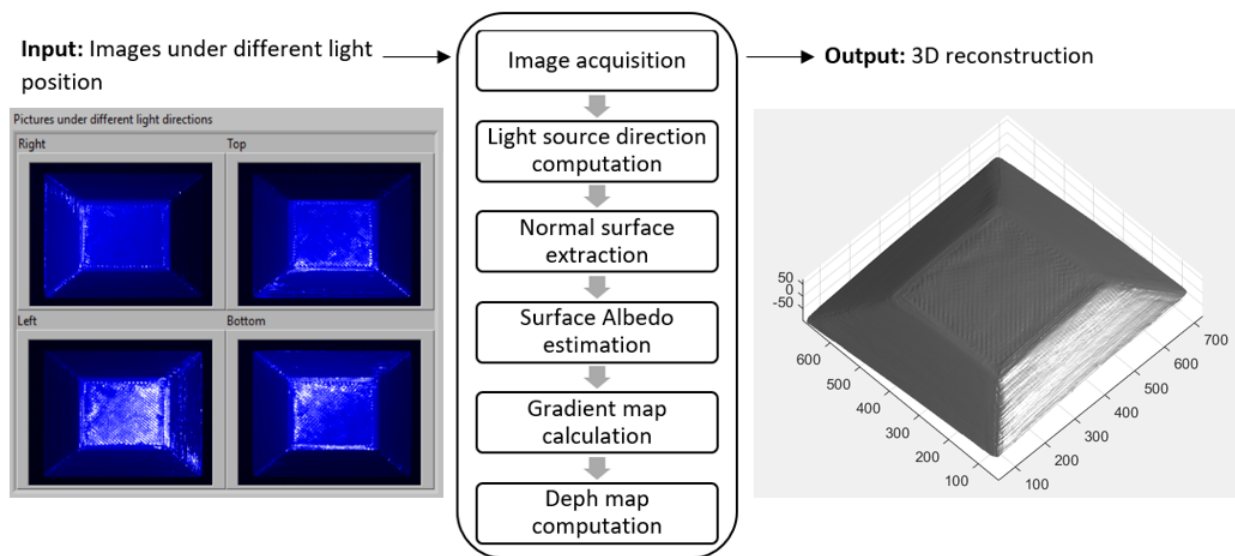


Figure 43 - Pipeline of the reconstruction program.

- **Decision making**

Finally, the decision-making phase consists of analyzing the result of the 3D reconstruction and determining whether the product meets the quality requirements or not, for example, checking whether the product has cracks, etc.

**4.3. Components for the optical evaluation**

The project design (see Figure 44) is composed of a camera, a light ring with 4-segment lights, the controller of the ring light, and the computer where the application is running.

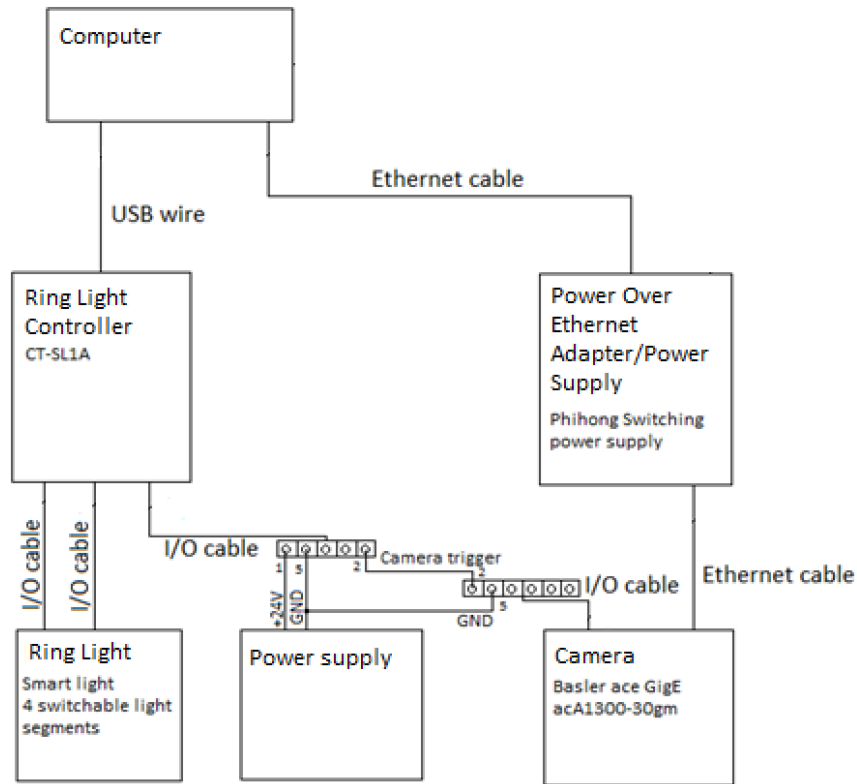


Figure 44 – Physical diagram of the solution model.

### 4.3.1. Camera

To elaborate this master thesis, it was necessary to find a suitable camera that allows obtaining a good quality in the images at the time of the obtaining process, but this requirement was not only considered when choosing the Basler ace GigE camera of reference acA1300-30gm (See Figure 45). The requirements to choose the camera were:

- This type of camera allows the possibility of modifying the exposure time at the time of capture, so it is a great advantage since reducing that time allows the camera sensor to not be saturated at the time of taking the image when the light is on.
- Modifying the size of the image to be captured, allows the image processing to be much faster since the number of pixels to be processed is reduced.
- As it is required to perform synchronization between the taking of images when a segment of the light ring is turned on, this camera allows modifying the parameters for the image taking, such as trigger mode, a parameter that allows an external signal to control the camera and take the image, for example, when the rising edge is detected.



Figure 45 - Basler ace GigE acA1300-30gm camera. [28]

Table 5 - Camera parameters. [28]

Camera parameter		Value
<b>Sensor</b>	Sensor vendor	Sony
	Sensor	ICX445
	Shutter	Global Shutter
	Max. Image circle	1/3"
	Sensor type	CCD
	Sensor size	4.9 mm x 3.6 mm
	Resolution (HxV)	1296 px x 966 px
	Resolution	1.3 MP
	Pixel size (HxV)	3.75 $\mu\text{m}$ x 3.75 $\mu\text{m}$
	Frame rate	30 fps
	Mono/Color	Mono
<b>Camera Data</b>	Interface	GigE
	Pixel Bit Depth	12 bits
	Synchronization	<ul style="list-style-type: none"> <li>• Hardware trigger</li> <li>• Free – run</li> <li>• Ethernet connection</li> </ul>
	Exposure control	<ul style="list-style-type: none"> <li>• Programmable via the camera API</li> <li>• Hardware trigger</li> </ul>
	Digital input	1
	Digital output	1
	Power supply	PoE or 12 VDC
	Power requirements (typical)	2.2 W
	Power consumption PoE	2.7 W

### 4.3.2. Illumination

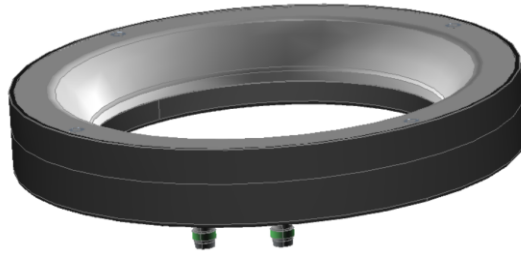


Figure 46 - Ring smart light. [29]

As can be seen in Figure 42, a ring light type of light source is used in the prototype design. Specifically, the model called Smart Light (see Figure 46), a device produced by the company Smart View that consists of 4 switchable light segments, capable of programming through the USB interface.

Table 6 - Ring light parameters. [29]

Ring light parameter	Value
Model series	SL-120W
Active illumination area	120 mm
Wavelength	CTR 5000 k
Voltage span ( $U_n$ )	7 – 28 V
Nominal voltage ( $U_{Im}$ )	24 V DC
Nominal current ( $I_{Im}$ )	625 mA
Single-segment current ( $I_{max}$ )	625 mA
Input ( $P$ )	15 W
Trigger voltage ( $U_{trig}$ )	$\geq 10 - 24$ V
Trigger current ( $I_{trig}$ )	2,3 mA
Analog light intensity regulation ( $U_{EN}$ )	$> 2,7 \dots \leq 10$ V
PWM light intensity regulation ( $U_{EN}$ )	$> 10$ V ... $\leq 24$ V
Segment input voltage S1-S4 ( $U_{seg}$ )	12 – 24 V
Segment input current S1-S4 ( $I_{seg}$ )	4 mA
A outer $\phi$ (mm)	172
B inner $\phi$ (mm)	120
C height (mm)	27,5
Active lighting area	$\phi$ mm
Weight	370 g

The ring light contains a controller that allows the connection of the computer with the ring of light, to give the possibility of modifying the different parameters that control the sequence of lights (for example, type of shot, frame time, etc. – see Figure 47).

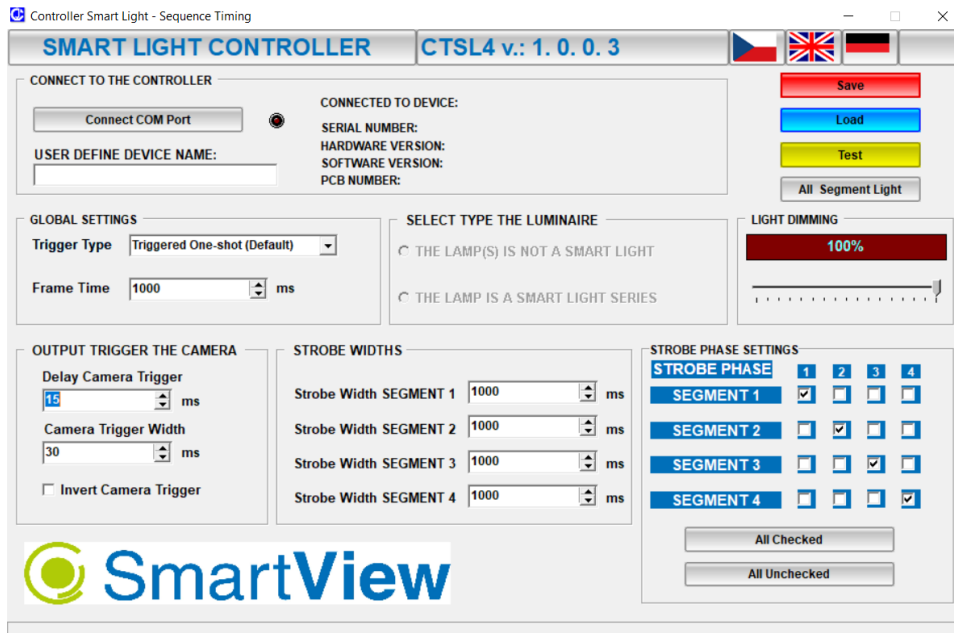


Figure 47 - The user application for setting the ring light parameters.

## 5. Software design for the visual inspection of industrial product

As described in the previous chapter, the system consists of three block diagrams with different functions during the inspection process, where each of the implemented components with their respective connections can be seen in Figure 44. Each task consists of an algorithm that can be represented by a flowchart that represents workflows from start to finish.

### 5.1. Image acquisition program

The image acquisition program oversees receiving the order from the user to start the image-taking process, when this order is activated, the program sends a command to the light controller to start the sequence and take the images under different light directions (see Figure 48).

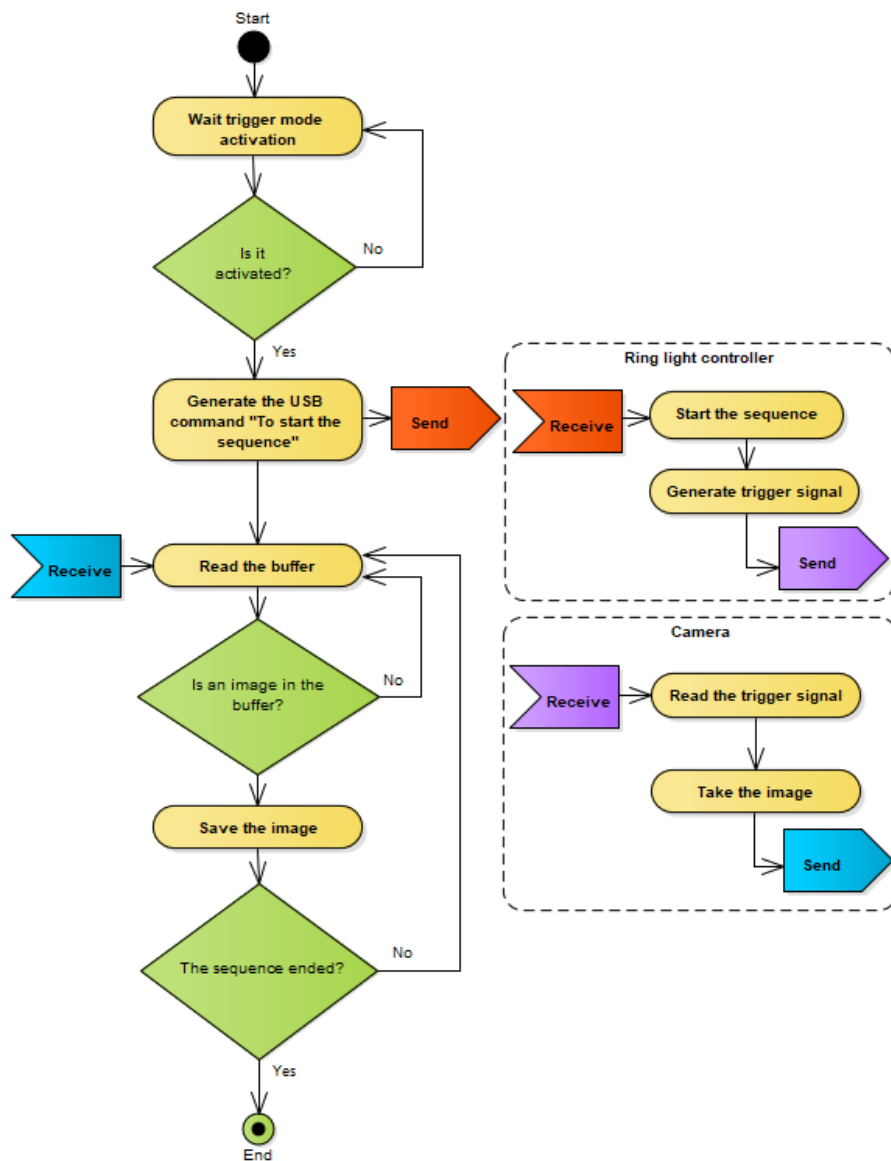


Figure 48 - Activity diagram of image acquisition.

- **Communication between the main program to the light controller**

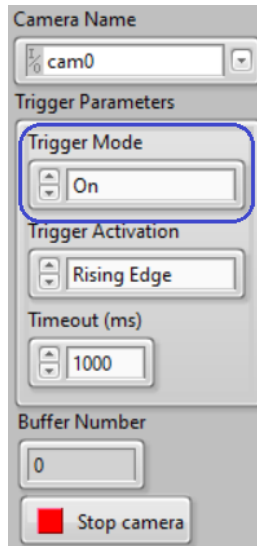


Figure 49 - Panel for activating the process of taking pictures.

When the user changes the camera's trigger mode parameter, a parameter that oversees activating the taking of images through an input signal (see Figure 49). In this case, the image is acquired when a rising edge is detected. The program sends a command to the light controller through USB communication, in this case, a string "T" command is sent in charge of letting the controller know to start the sequence of lights (see Figure 50).

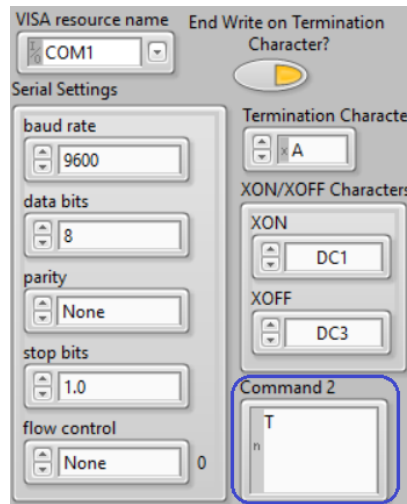


Figure 50 - USB configuration Panel.



- **Light and Camera synchronization**

The synchronization between the process of taking the images and the sequence of lights flashes was carried out by using the signal generated by the ring light when each segment is turned on (see Figure 51), the signal that is connected to the input trigger signal of the camera (see Figure 44).

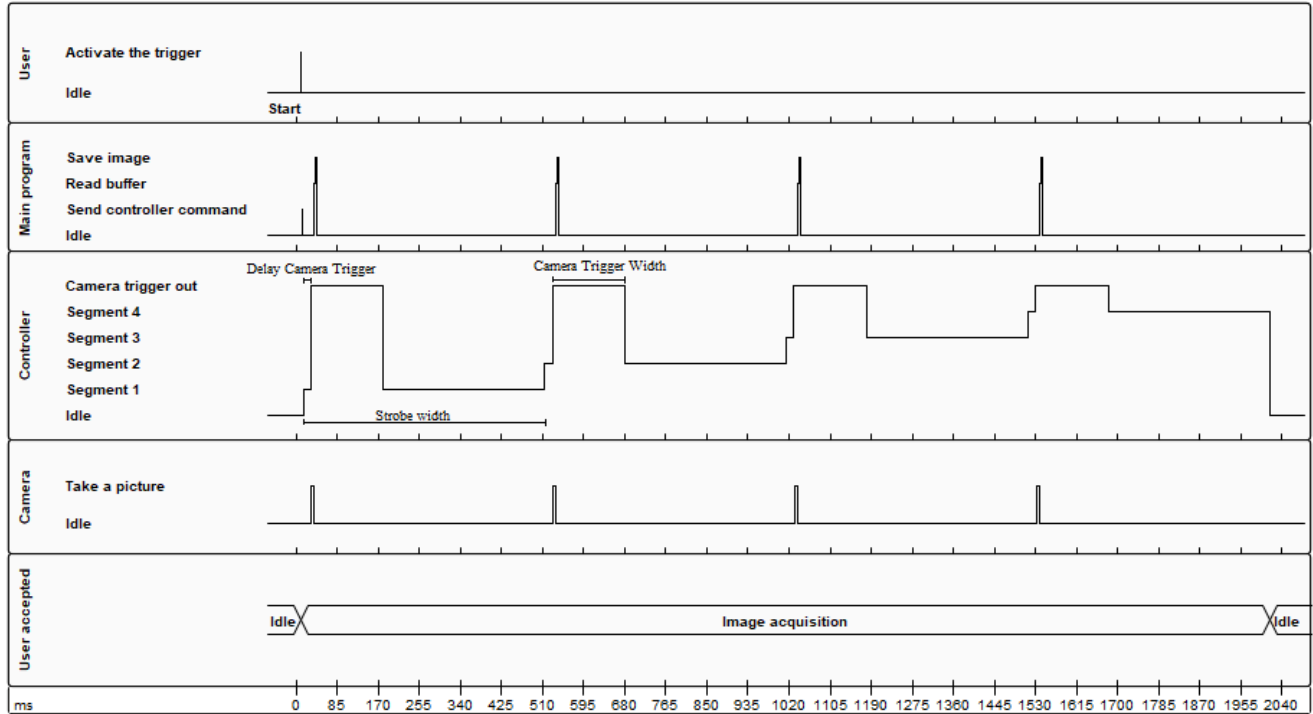


Figure 51 - Timing diagram for image acquisition.

The signal is composed by:

- Delay camera trigger: time between turning on the segment light and the rising edge to trigger the camera.
- Camera trigger width: time that describes how long the camera trigger signal will remain at a high level.
- Strobe width: the time each segment will stay on.

**5.2. 3D reconstruction algorithm**

After obtaining the images, we proceed to obtain the directions of the light source, a result obtained after the calibration. When these input parameters are present, the surface mask is calculated, the mask that separates the surface of interest, in this case, the object to be inspected concerning the base (see Figure 52).

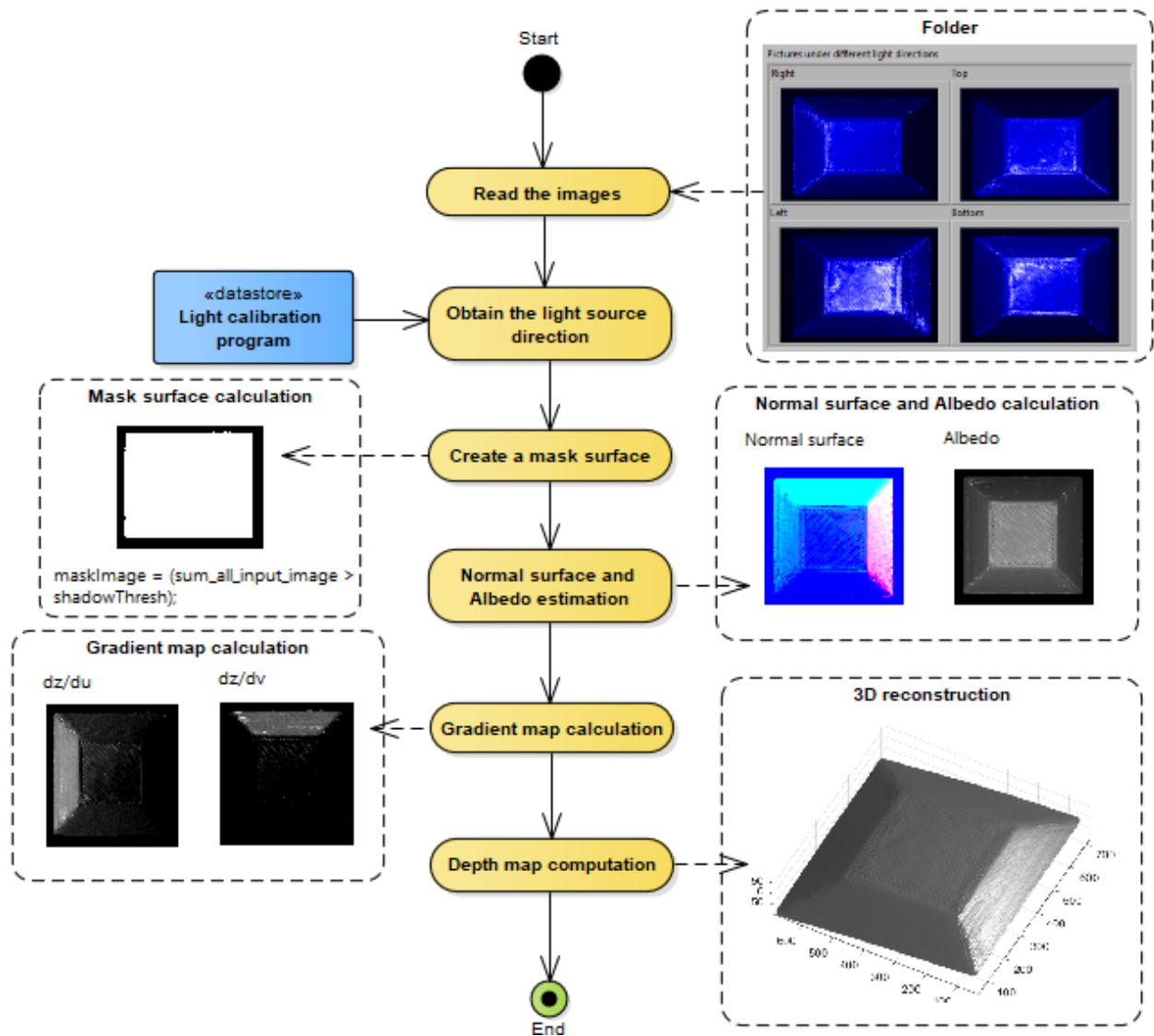


Figure 52 - Activity diagram for 3D reconstruction program.

After obtaining the mask, it allows the program to determine from which pixel coordinates the algorithm begins to calculate the surface of interest, in this case, the normal surface is generated, a surface that shows the vectors perpendicular to the tangent plane of the surface and the surface Albedo, characteristic that represents the amount of incident radiation that is reflected through the surface of the object (See Figure 52).

The process for obtaining these two surfaces is carried out by using Eq. 8, where a new variable is assigned to the multiplication of the albedo surface and the normal surface, called  $G(x, y)$ .

$$I = L^T \underbrace{\lambda N^T}_{G(x,y)} = \left( \underbrace{\lambda N^T}_{G(x,y)} \right)^T L \quad \text{Eq. 22}$$

Solving the equation to find the value of  $G(x, y)$  using the given pixel provides Eq. 23

$$G(x, y) = (L^T L)^{-1} L^T \cdot I(x, y) \quad \text{Eq. 23}$$

finally, using Eq. 23 it is possible to calculate the albedo surface (Eq. 24) and the normal surface (Eq. 25), formulas implemented in the algorithm designed in LabVIEW.

$$\lambda(x, y) = \|G(x, y)\| \quad \text{Eq. 24}$$

$$N(x, y) = \frac{G(x, y)}{\lambda} \quad \text{Eq. 25}$$

by obtaining these two surfaces, the gradient map can be calculated, a map composed of a set of 3D points  $[x(u, v), y(u, v), z(u, v)]$ . Assuming  $x$  and  $y$  are orthogonal to the camera view, the normal surface can be specified depending on the depth partial derivatives (Eq. 26).

$$N(u, v) \propto \left[ \frac{\partial z(u, v)}{\partial u}, \frac{\partial z(u, v)}{\partial v}, -1 \right]^T \quad \text{Eq. 26}$$

Through mathematical processes and the implementation of auxiliary variables, the equations necessary to calculate these gradients are obtained:

$$p = \frac{\partial z}{\partial u} = -\frac{n_1}{n_3} \quad \text{Eq. 27}$$

$$q = \frac{\partial z}{\partial v} = -\frac{n_2}{n_3} \quad \text{Eq. 28}$$

To calculate the surface having the gradients, it must be guaranteed that the partial derivatives must be integrable, but errors or noise may occur during the process. An alternative is proposed to carry out the integration process of these gradients using the Frankot and Chellappa method [30], this method oversees approximating the best signal that describes the differential curves, in this case using Fourier transform.

$$z(u, v) = F^{-1} \left( \frac{j\omega_u F(p(u, v)) + j\omega_v F(q(u, v))}{\omega_u^2 + \omega_v^2} \right) \quad \text{Eq. 29}$$

So each of the equations described above was implemented to build the following algorithm implemented in LabVIEW – see Figure 53.

**3D reconstruction**  
 After the images are obtained, the 3D reconstruction is carried out, a procedure that consists of extracting the normal surface and the Albedo surface depending on the positions of the lighting direction, when these two surfaces are calculated, we proceed to calculate the gradients, variable that will allow the computation of the depth map.

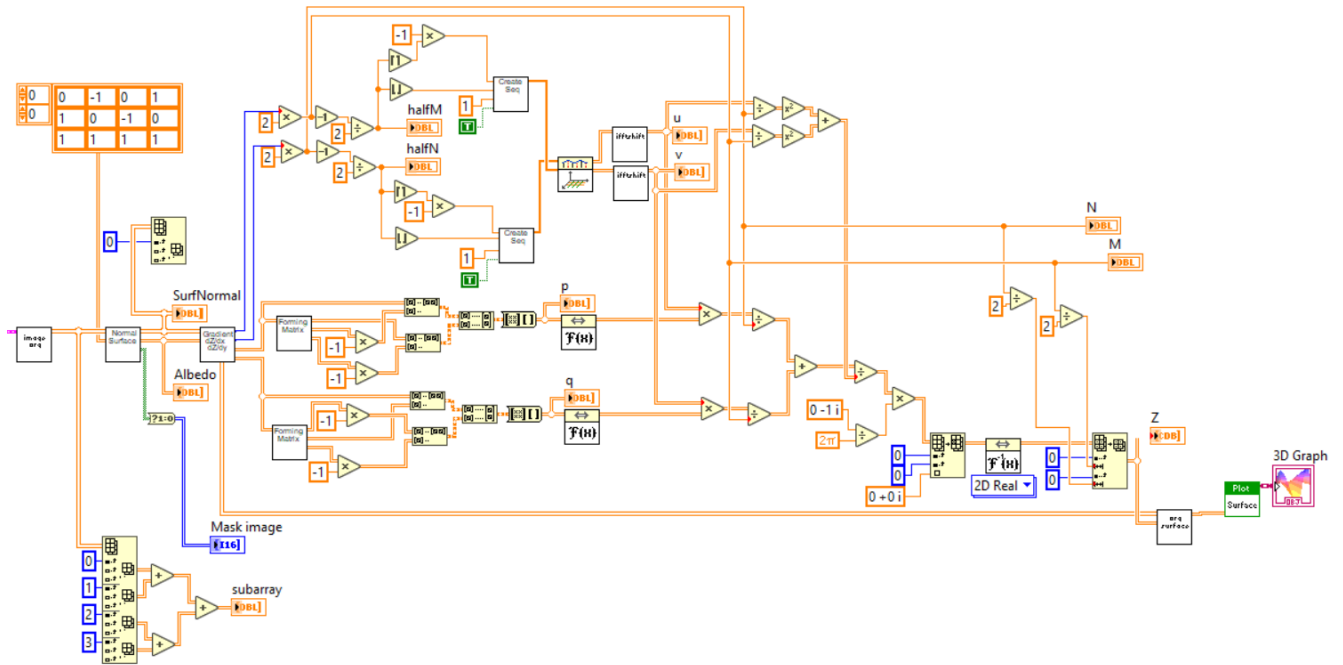


Figure 53 - 3D reconstruction program designed in LabVIEW.

### 5.3. Light direction calculation

To calculate the normal surface and the albedo surface, it is necessary to obtain the direction of each of the light segments. That is why a program was developed capable of finding the highlight point and calculating its position within the region of the sphere.

#### 1. Fitting light probe circle

The first step is to estimate the circle that corresponds to the test sphere (see Figure 54).

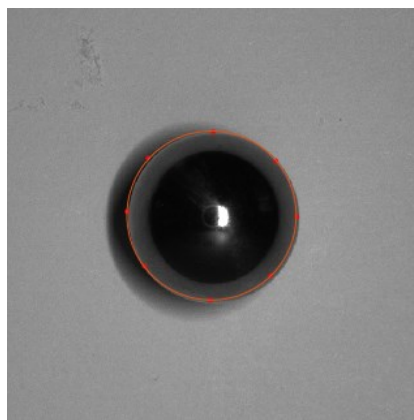


Figure 54 - Fitting light probe circle.

## 2. Calculate the centroid and radius

When testing the circle, we proceed to find the center of it and calculate the radius, parameters necessary to be able to define the locations of each segment of light.

## 3. Finding light direction

After obtaining the parameters that make up the circle, we proceed to estimate the location of the highlight point using the following equation (see Figure 55)

$$L = 2(N \cdot R)N - R \quad \text{Eq. 30}$$

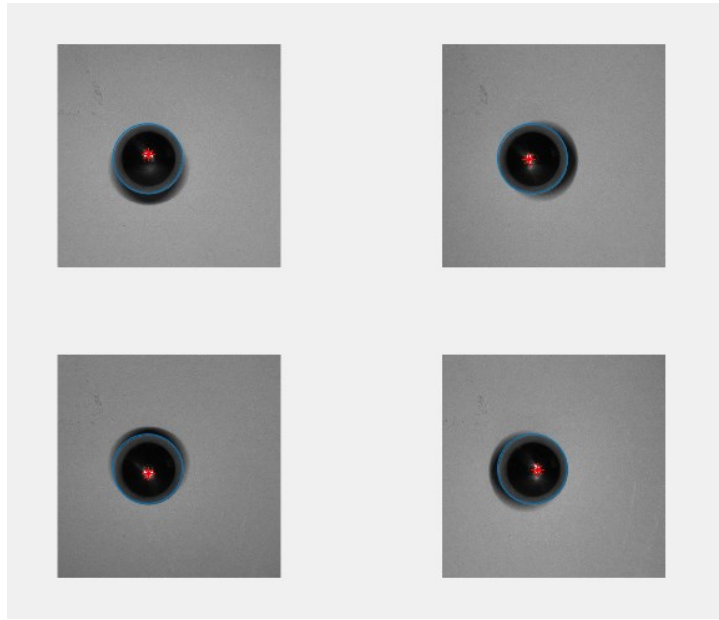


Figure 55 - Finding light direction.

where the normal vector is calculated for each component concerning the center to the highlight point and  $R$  is the direction of the camera to  $C = [0 \ 0 \ 1]^T$ .

$$N_x = \frac{x_h - x_c}{r} \quad \text{Eq. 31}$$

$$N_y = \frac{y_h - y_c}{r} \quad \text{Eq. 32}$$

$$N_z = \sqrt{1 - x^2 - y^2} \quad \text{Eq. 33}$$

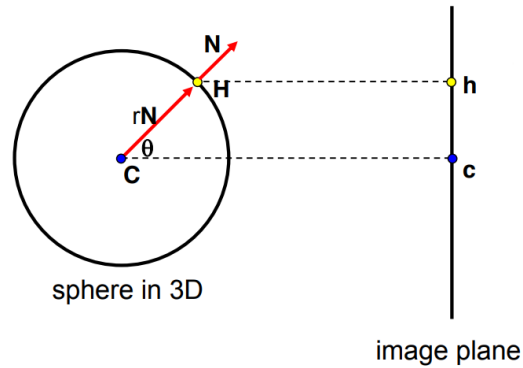


Figure 56 - Graphic representation of the sphere with a highlight at point H.

#### 5.4. Camera calibration

After obtaining the 3D reconstruction of the object, the main objective is to carry out an inspection, in this case, to measure the dimensions of the object. we proceed to carry out the calibration of the camera to find the necessary parameters to carry out the conversion of pixels to real units, for example, centimeters.

To perform this calibration, a chess pattern (see Figure 57) is used, which will first be placed on the base and then at different angles of inclination to obtain the intrinsic and extrinsic parameters of the camera.

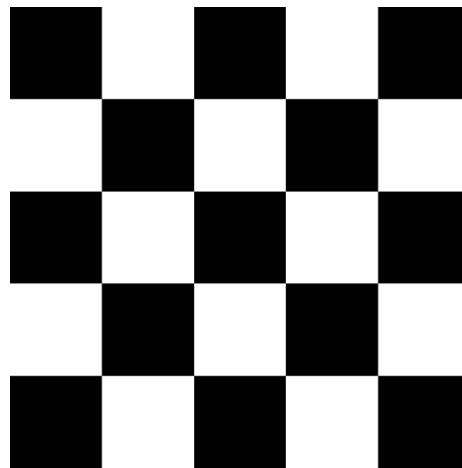


Figure 57 - Chessboard pattern.

##### - Intrinsic parameters

The intrinsic parameters oversee defining the geometry of the internal and optics of the camera, some of these parameters are:

- The focal length ( $f$ ), the distance between the lens concerning the principal point (see Figure 58).
- The principal point ( $Cx, Cy$ ), point of intersection between the plane of the camera image and optical axis (see Figure 58).

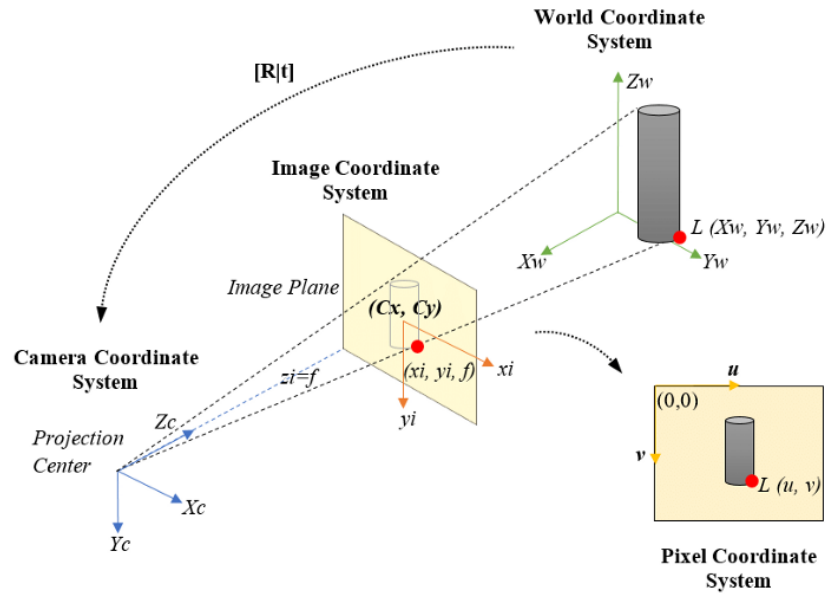


Figure 58 - Camera projection model.

- **Extrinsic parameters**

The extrinsic parameters of the camera oversee relating the coordinate system of the real world concerning the camera, that is, these parameters describe the position and orientation of the camera concerning the coordinates of the real world (see Figure 59).

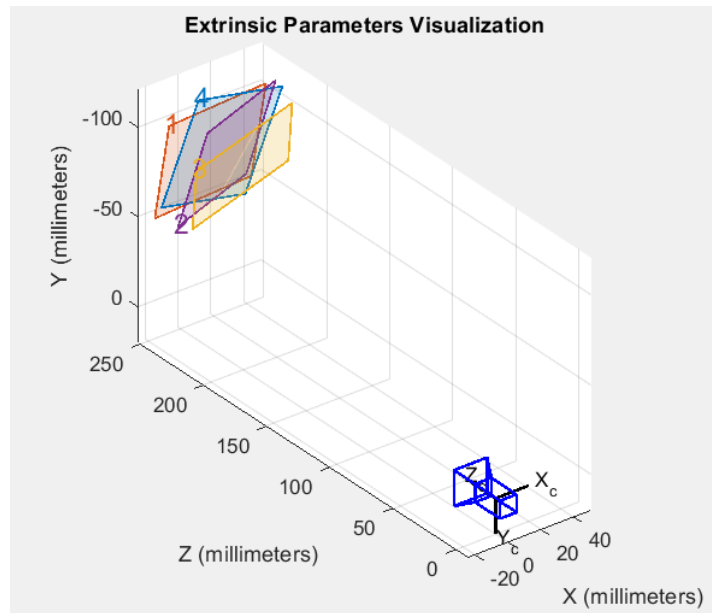
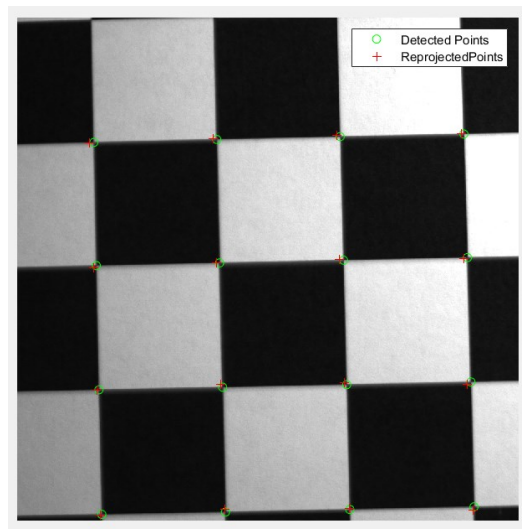


Figure 59 - Extrinsic parameters visualization.

To verify the results obtained by calibrating the camera, the following measurements can be made from the model designed for capturing images. The distance in millimeters between the camera concerning the base was obtained by using a ruler capable of measuring the distance between these two points. This result was compared with the extrinsic parameter of the position generated by the calibration system. In the same way, it was possible to verify the angle of inclination of the camera, but unlike the previous parameter, this was obtained by implementing a clinometer and thus comparing this result with the extruded orientation parameter obtained by the calibration.

#### 5.4.1. Pixel to real unit conversion for X and Y-axis

For the conversion of pixels to real units concerning the x and y-axis, one of the results obtained by calibrating the camera is used. Said result consists in that the algorithm detects the corners of the squares (see Figure 60) and when obtaining them makes the equivalence between pixels and the real units since the distance between the sides of the squares is known.



*Figure 60 - Detected and reprojected points from chessboard pattern.*

This equivalence consists of finding a scaling factor, which is going to be multiplied by the range of pixels obtained from each of the axes.



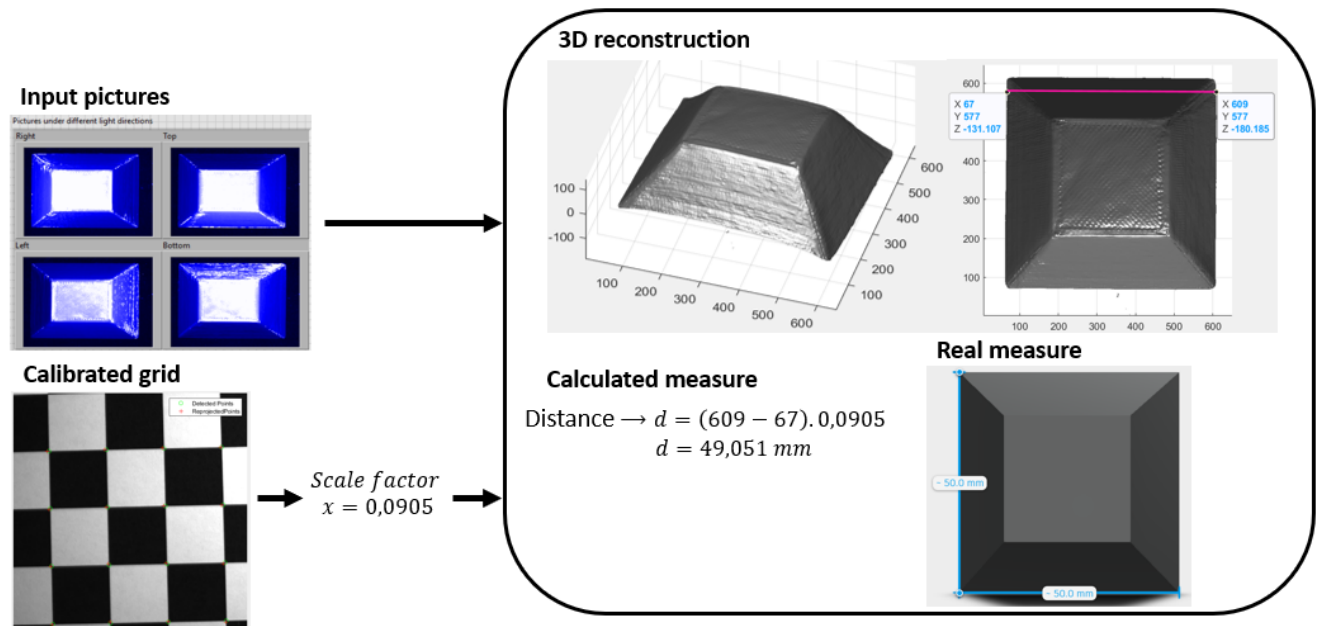


Figure 61 - Process of conversion from pixel to real units

#### 5.4.2. Pixel to real unit conversion for Z-axis

For the z-axis calibration, a known measurement is used, in this case, the height of the inspection object, which will be taken as a reference to build a new range, which will be implemented on the surface and thus dimensioned according to the real units.

To perform this conversion process

1. The height measurement of the real object is taken.

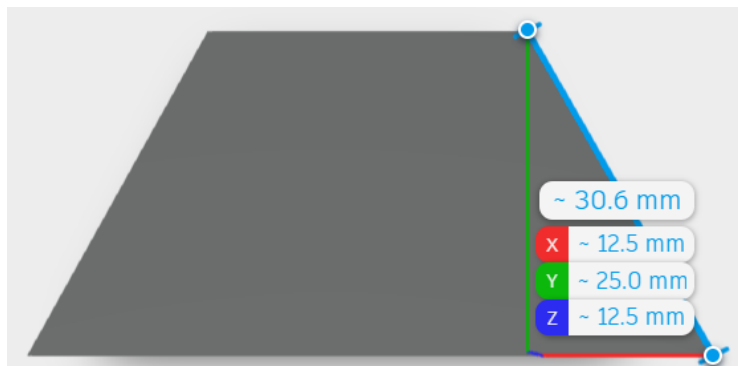


Figure 62 - Real height measured.

2. The maximum point of the obtained surface is found.
3. Find the scale factor that relates to how much a 1 pixel equals in real units.

For example, the maximum value is 225.816 pixels, so the scale factor is calculated as:

$$\text{Scale factor} = \frac{25}{225,816} = 0.1107$$

4. The scale factor is multiplied to the range of the z-axis generated by the reconstruction.

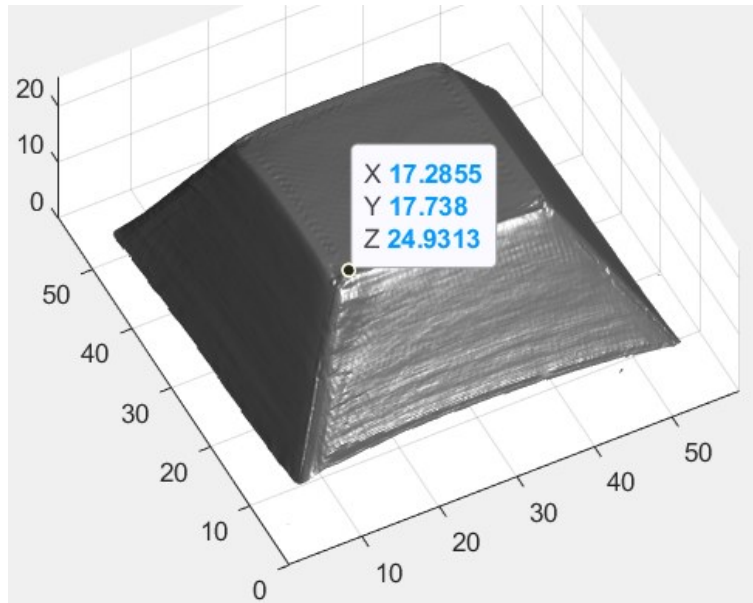


*Figure 63 - Z-axis after multiplying by the scale factor (X and Y axis are calibrated).*

## 6. Evaluation of the achieved results

After implementing the necessary calibrations, the inspection process was carried out on different objects that differ in geometry, material, or dimensions, to analyze the response of the system. The results analysis process was carried out by comparing the results obtained through the reconstruction and the actual measurements of the object.

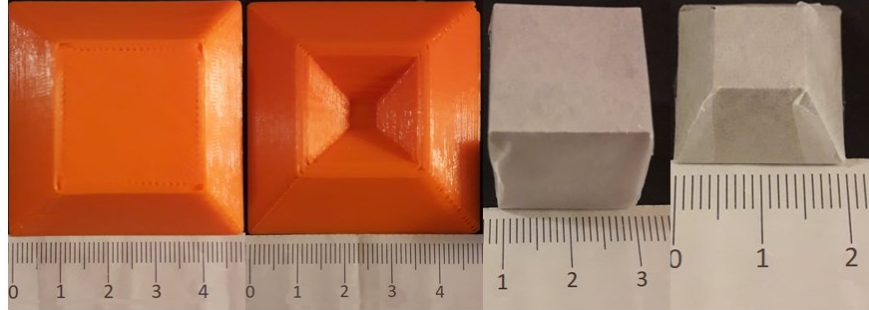


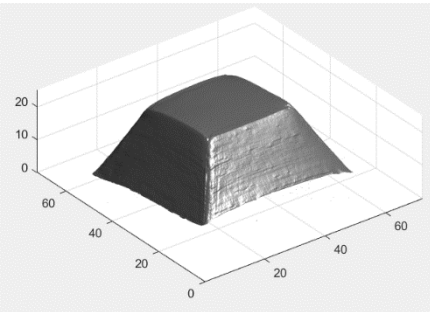
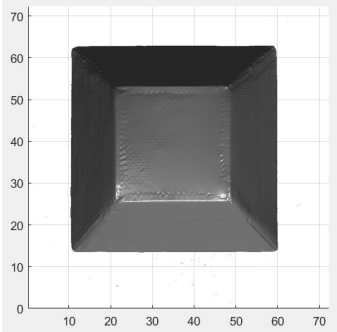
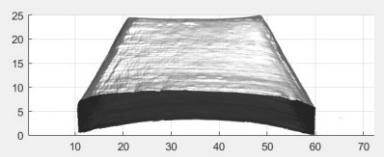
Figure 64 - Example of how the measurement of the real measure was performed.

The calculation of the error was carried out using the following equation

$$\text{error}(\%) = \left| \frac{\text{Real}_{\text{Measurement}} - \text{Reconstruction}_{\text{Measurement}}}{\text{Real}_{\text{Measurement}}} \right| \times 100\% \quad \text{Eq. 34}$$

- **Pyramid with dimensions of 50mm x 50mm x 25mm (width, length, height)**

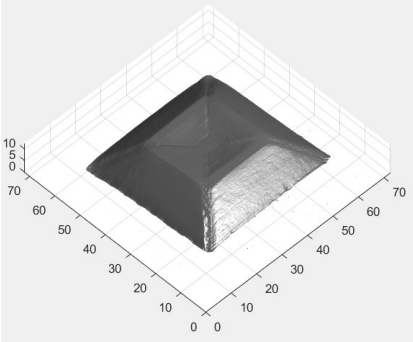
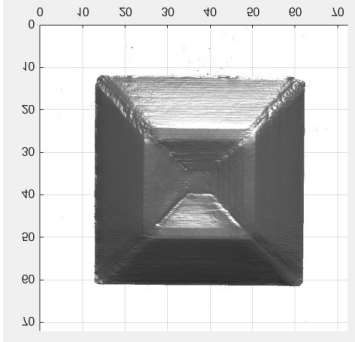
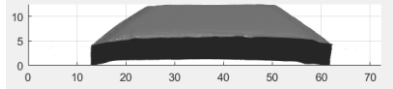
Table 7 - 3D reconstruction for a pyramid with dimensions of 50mm x 50mm x 25mm.

Pyramid		
3D view	XY view	XZ view
		
Measurement	Value	Error
Width	49,4130 mm	1,1740%
Length	48,9605 mm	2,0790%
Height	24,1958 mm	3,2168%

In addition to analyzing the dimensions, it was also considered to see how the system can perform a 3D reconstruction of an element that presents a little more detail on its surface (see Table 8), so it can be seen that the system manages to define each one of the details present in the object to be analyzed, which opens the opportunity to later implement the algorithm in a component or deformity inspection process, an example of this is the weld inspection.

- **Pyramid with dimensions of 50mm x 50mm x 12,5mm (width, length, height)**

*Table 8 - 3D reconstruction for a pyramid with dimensions of 50mm x 50mm x 12,5mm.*

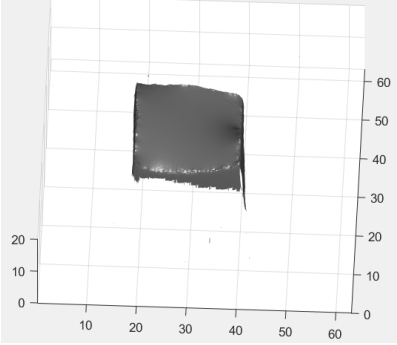
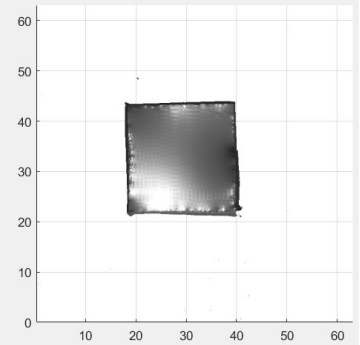
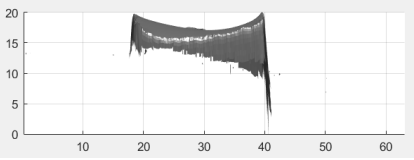
Pyramid		
<b>3D view</b>	<b>XY view</b>	<b>XZ view</b>
		
Measurement	Value	Error
<b>Width</b>	48,8700 mm	2,2600%
<b>Length</b>	48,8700 mm	2,2600%
<b>Height</b>	12,3785 mm	0,9720%

Another object that was used to check the precision of the program was a cube, but it was observed that with this figure the reconstruction was not carried out, it was simply possible to extract the upper part of the cube, this is because, from the perspective from where the camera is, it is not possible to see each face that composed the figure (see Table 9).

It should be noted that these last two figures (see Table 9 and Table 10) were covered with matte paper to create a Lambertian surface since before the light that is incident was not reflected uniformly.

- **Cube 20mm x 20mm x 20mm (width, length, height)**

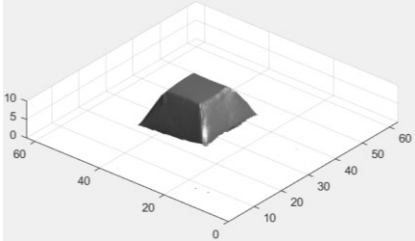
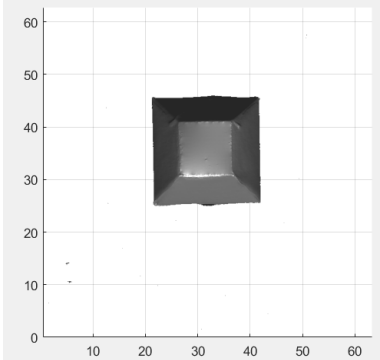
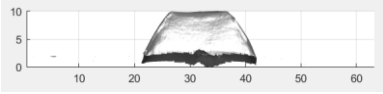
*Table 9 - 3D reconstruction for a cube with dimensions of 20mm x 20mm x 20mm.*

Cube		
<b>3D view</b>	<b>XY view</b>	<b>XZ view</b>
		
Measurement	Value	Error
Width	21,358 mm	6,7900%
Length	22,1725 mm	10,8625%
Height	----	---

Finally, a pyramid (see Table 10) with the same geometry as the first pyramid (see Table 7) was implemented but it differs in terms of dimensions, since it is much smaller, comparing these two results, the error in this last figure is much smaller than in the previous one. This is because the distance between the illumination lights, in this case, the light ring, can mark the depth of the object much more.

- Pyramid with dimensions of 20mm x 20mm x 10mm (width, length, height)

Table 10 - 3D reconstruction for a pyramid with dimensions of 20mm x 20mm x 10mm.

Pyramid		
<p style="text-align: center;"><b>3D view</b></p> 	<p style="text-align: center;"><b>XY view</b></p> 	<p style="text-align: center;"><b>XZ view</b></p> 
Measurement	Value	Error
<b>Width</b>	20,0005 mm	0,0025%
<b>Length</b>	19,8195 mm	0,9025%
<b>Height</b>	9,8525 mm	1,4750%

## Conclusion

To conclude, the system created using a four-segment light ring with its respective controller, a monochrome camera, and a laptop where the implemented program is located allows to obtain a good qualitative and quantitative precision of the inspected object. The core of this work was to understand Photometric Stereo principles, to learn how to deal with camera, to understand how to program the light controller, to program 3D vision algorithm in LabVIEW, and to understand and implement calibration of the whole system. Thus opening a wide range of opportunities to implement this algorithm in other types of applications or inspections.

The method of photometric stereo, based on the taking of several images under different lighting directions, to estimate the depth of the object, brings with it several advantages over other types of 3D reconstruction. It is only necessary to implement a camera in the system, thus lowering the economic costs. Another advantage is that the implemented algorithm is much more optimal in terms of processing time, due to the simplification of the algorithm routine.

Analyzing the results obtained from the different objects inspected, as previously stated, a good precision in the results was obtained, but also during the process of construction and testing of the system, certain limitations were found when applying the algorithm and obtaining a good quality on the reconstruction. One of those limitations is the reflectance index of the base of our system, in many cases while several measurements were taken, it could be observed that within the error percentage of the 3D reconstruction, it is because when the object is illuminated, some portion of the light is reflected from the base, so the algorithm takes that piece into account as part of the figure to be reconstructed. This limitation could be improved by implementing a camera that allows modifying the brightness and contrast parameters, to improve the difference between the lighter and darker colors, in the same way, this could open an opportunity to inspect shiny objects.

And finally, as future work to reduce the inaccuracy generated concerning the calibration of the axes by converting pixels to real units, a point cloud could be created from the surface map, to obtain the positions Three-dimensional of these points in space and thus ensuring accurate measurements, this point cloud technology can currently be found in 3D laser scanning.

## References

- [1] ZHANG, Yiwei. *Investigations into applications of photometric stereo and single-pixel imaging*. Glasgow, 2017. Doctoral thesis. University of Glasgow.
- [2] KALA, Rahul. *On-Road Intelligent Vehicles* [online]. Elsevier, 2016 [cit. 2020-11-01]. ISBN 9780128037294. Avalibale from: doi:10.1016/C2015-0-00389-6
- [3] LOGOTHETIS, Fotios. *Detailed and Practical 3D Reconstruction with Advanced Photometric Stereo Modelling* [online]. Cambridge, 2019 [cit. 2020-10-20]. Available from: <https://doi.org/10.17863/CAM.39609>. Doctoral thesis. University of Cambridge. Vedoucí práce Roberto Cipolla.
- [4] CIORA, Radu a Carmen SIMION. Industrial Applications of Image Processing. *ACTA Universitatis Cibiniensis* [online]. 2014, **64**(1), 17-21 [cit. 2020-12-22]. ISSN 1583-7149. Avalibale from: doi:10.2478/aucts-2014-0004
- [5] MISHRA, Vikas Kumar, Shobhit KUMAR a Neeraj SHUKLA. Image Acquisition and Techniques to Perform Image Acquisition. *SAMRIDDI: A Journal of Physical Sciences, Engineering and Technology* [online]. 2017, **9**(01), 21-24 [cit. 2020-12-30]. ISSN 2454-5767. Avalibale from: doi:10.18090/samriddhi.v9i01.8333
- [6] REAL, Fábio Dias a François BERRY. Smart Cameras: Technologies and Applications. BELBACHIR, Ahmed Nabil, ed. *Smart Cameras* [online]. Boston, MA: Springer US, 2010, s. 35-50 [cit. 2021-01-04]. ISBN 978-1-4419-0954-1. Avalibale from: doi:10.1007/978-1-4419-0953-4\_3
- [7] MHD ZAFER AL HOSNY, Mouaz. *Basic description of CMOS camera sensor and color precnible* [online]. In: . s. 6 [cit. 2021-01-06]. Avalibale from: doi:10.13140/RG.2.2.20644.48008
- [8] *VISoc: A smart camera SoC* [online]. In: ALBANI, L, P CHIESA, Daniele COVI, G PEDEGANI, A SARTORI a Monica VATTERONI. Trento, Italy: IEEE Xplore, 2002, s. 367-370 [cit. 2021-01-17]. Avalibale from: [https://www.researchgate.net/publication/4158259\\_VISoc\\_A\\_smart\\_camera\\_SoC](https://www.researchgate.net/publication/4158259_VISoc_A_smart_camera_SoC)
- [9] RINNER, B. a W. WOLF. An Introduction to Distributed Smart Cameras. *Proceedings of the IEEE* [online]. 2008, **96**(10), 1565-1575 [cit. 2021-01-17]. ISSN 0018-9219. Avalibale from: doi:10.1109/JPROC.2008.928742
- [10] GenICam. *Opto Engineering* [online]. Opto Engineering, 2019 [cit. 2021-01-17]. Avalibale from: <https://www.opto-e.com/basics/genicam-standard>
- [11] Lighting. *Opto Engineering* [online]. Opto Engineering, 2019 [cit. 2021-01-23]. Avalibale from: <https://www.opto-e.com/basics/lighting>



- [12] LED illumination. *Opto Engineering* [online]. Opto Engineering, 2019 [cit. 2021-01-23]. Available from: <https://www.opto-e.com/basics/led-illumination>
- [13] MACISAAC, Dan, Gary KANNER a Graydon ANDERSON. Basic physics of the incandescent lamp (lightbulb). *The Physics Teacher* [online]. 1999, **37**(9), 520-525 [cit. 2021-01-23]. ISSN 0031-921X. Available from: doi:10.1119/1.880392
- [14] Fluorescent Lamp and Working Principle of Fluorescent Lamp. *Electrical 4 U* [online]. Electrical 4 U, 2020 [cit. 2021-01-23]. Available from: <https://www.electrical4u.com/fluorescent-lamp-its-working-principle/>
- [15] LED (LIGHT-EMITTING DIODES). *Trilux simplify your light* [online]. Trilux [cit. 2021-01-23]. Available from: <https://www.trilux.com/en/lighting-practice/lighting-equipment/light-sources/light-source-types/led-light-emitting-diodes/>
- [16] IMAQ: IMAQ Vision for LabVIEW™ User Manual. In: *IMAQ: IMAQ Vision for LabVIEW™ User Manual*. June 2003. National Instruments, 2003, s. 131.
- [17] SZELISKI, Richard. *Computer Vision: Algorithms and Applications*. London: Springer, 2010. Texts in computer science. ISBN 978-1-84882-934-3.
- [18] VOUDOUKIS, Nikolaos a Sarantos OIKONOMIDIS. Inverse square law for light and radiation: A unifying educational approach. *European Journal of Engineering Research and Science* [online]. 2017, **2**(11), 23-27 [cit. 2020-11-03]. ISSN 2506-8016. Available from: doi:10.24018/ejers.2017.2.11.517
- [19] BALSKEY, Marek a Jiri HABEL. Measurement and Recording of Reflective Properties of Materials. In: *Proceedings of the 21st International Conference LIGHT SVĚTLO 2015* [online]. Brno: Fakulta elektrotechniky a komunikacních technologií VUT v Brně, 2015, s. 263-266 [cit. 2020-11-03]. ISBN 978-80-214-5244-2. Available from: doi:10.13164/conf.light.2015.263
- [20] PÉREZ-RODRÍGUEZ, Ángel Luis, Guadalupe MARTÍNEZ-BORREGUERO a María Isabel SUERO-LÓPEZ. New didactic formulation of the laws of reflection of light. *Revista Brasileira de Ensino de Física* [online]. 2017, **39**(2) [cit. 2020-11-03]. ISSN 1806-1117. Available from: doi:10.1590/1806-9126-rbef-2016-0272
- [21] TANG, Yichuan, Ruslan SALAKHUTDINOV a Geoffrey HINTON. Deep Lambertian Networks. In: *Deep Lambertian Networks* [online]. ICML, 2012, s. 8 [cit. 2021-02-07]. Available from: <https://arxiv.org/ftp/arxiv/papers/1206/1206.6445.pdf>

- [22] COAKLEY, J.A. REFLECTANCE AND ALBEDO, SURFACE. *Encyclopedia of Atmospheric Sciences* [online]. Elsevier, 2003, s. 1914-1923 [cit. 2020-11-03]. ISBN 9780122270901. Available from: doi:10.1016/B0-12-227090-8/00069-5
- [23] KIM, Jihun, Hasan AL FARUQUE, Sewoong KIM, Eunjoo KIM a Jae Youn HWANG. Multimodal endoscopic system based on multispectral and photometric stereo imaging and analysis. *Biomedical Optics Express* [online]. 2019, **10**(5) [cit. 2020-12-06]. ISSN 2156-7085. Available from: doi:10.1364/BOE.10.002289
- [24] CRISPEL, Pierre a Gregory ROBERTS. All-sky photogrammetry techniques to georeference a cloud field. *Atmospheric Measurement Techniques* [online]. 2018, **11**(1), 593-609 [cit. 2021-02-07]. ISSN 1867-8548. Available from: doi:10.5194/amt-11-593-2018
- [25] BATTIATO, Sebastiano, Brian D. CORNER, Peng LI, Salvatore CURTI, Marco LA CASCIA, Roy P. PARGAS, Marcello TORTORA a Emiliano SCORDATO. *Depth map generation by image classification* [online]. In: . s. 95- [cit. 2020-12-09]. Available from: doi:10.1117/12.526634
- [26] QIAN, Yan, Ruiqing HE, Qian CHEN, Guohua GU, Feng SHI a Wenwen ZHANG. Adaptive compressed 3D ghost imaging based on the variation of surface normals. *Optics Express* [online]. 2019, **27**(20) [cit. 2020-10-20]. ISSN 1094-4087. Available from: doi:10.1364/OE.27.027862
- [27] ZHANG, Yiwei, Graham M. GIBSON, Rebecca HAY, Richard W. BOWMAN, Miles J. PADGETT a Matthew P. EDGAR. A fast 3D reconstruction system with a low-cost camera accessory. *Scientific Reports* [online]. 2015, **5**(1) [cit. 2020-10-20]. ISSN 2045-2322. Available from: doi:10.1038/srep10909
- [28] AcA1300-30gm - Basler ace. *BASLER the power of sight* [online]. Basler web [cit. 2021-02-07]. Available from: <https://www.baslerweb.com/en/products/cameras/area-scan-cameras/ace/aca1300-30gm/>
- [29] SMART LIGHT. *Smart View* [online]. Smart View [cit. 2021-02-07]. Available from: <https://www.smartview.cz/>
- [30] A New Algorithm for Gradient Field Integration. In: WEI, Tiangong a Reinhard KLETTE. *A New Algorithm for Gradient Field Integration*. Dunedin, 2001, s. 8.